NASA Contractor Report 198294

ICASE Report No. 96-17

ICASE

DESCRIPTION OF JET BREAKUP

Demetrios T. Papageorgiou

NASA Contract No. NAS1-19480
March 1996

Institute for Computer Applications in Science and Engineering
NASA Langley Research Center
Hampton, VA 23681-0001

Operated by Universities Space Research Association

National Aeronautics and
Space Administration

Langley Research Center
Hampton, Virginia 23681-0001

DESCRIPTION OF JET BREAKUP

Demetrios T. Papageorgiou[1]
Department of Mathematics
Center for Applied Mathematics and Statistics
New Jersey Institute of Technology
Newark, NJ 07102

Abstract

In this article we review recent results on the breakup of cylindrical jets of a Newtonian fluid. Capillary forces provide the main driving mechanism and our interest is in the description of the flow as the jet pinches to form drops. The approach is to describe such topological singularities by constructing local (in time and space) similarity solutions from the governing equations. This is described for breakup according to the Euler, Stokes or Navier-Stokes equations. It is found that slender jet theories can be applied when viscosity is present, but for inviscid jets the local shape of the jet at breakup is most likely of a non-slender geometry. Systems of one-dimensional models of the governing equations are solved numerically in order to illustrate these differences.

[1]This work was supported by the Air Force Office for Scientific Research Grant (F49620-94-1-0242) and the National Science Foundation (Grant DMS 9-9-0070). Additional support was also provided by the National Aeronautics and Space Administration under NASA Contract No. NAS1-19480 while the author was in residence at the Institute for Computer Applications in Science and Engineering (ICASE), NASA Langley Research Center, Hampton, VA 23681-0001

1 Introduction

A perfectly cylindrical column of fluid at rest is an exact solution of the governing equations whether viscosity is included or not. When surface tension acts, this configuration is unstable to long waves due to capillary instability; any small perturbation with wavelength larger than the undisturbed jet radius is unstable. These linear solutions were first given by Rayleigh's pioneering studies in capillary instability, see for example Rayleigh [17], [23]. For inviscid jets, for instance, Rayleigh calculated the most unstable wave to have wavelength approximately nine times the jet radius. Even though breakup into drops is a nonlinear phenomenon linear theory does surprisingly well in predicting overall features such as drop sizes and breakup times. For a quantitative description of breakup linear theory must be abandoned and we shall be exclusively concerned with nonlinear solutions here.

This classical problem has received considerable attention over the years. Experimental work has been carried out by Donnelly and Glaberson [10], Goedde and Yuen [15] and more recently by Chaudhary and Maxworthy [7], [8]. The related problem of the dripping faucet was studied by Hauser et al. [16] and in much more detail by the recent work of Peregrine, Shoker and Symon [31] and [40], [3] where sequences of photographs detailing the breakup can be found. The latter authors report on a fascinating cascading phenomenon during pinching.

Theoretical studies including nonlinear effects are more recent and roughly fall into three categories: Direct numerical simulations, weakly nonlinear theories and slender jet theories. Since we will be concerned with both inviscid and viscous flows the literature is reviewed separately.

For inviscid jets, theories stemming from the classical weakly nonlinear approach of Stuart [42] and Watson [46], have been applied by Yuen [48], Chaudhary and Redekopp [9] and Lafrance [21]. These approaches follow the evolution of two low amplitude initial perturbations, a fundamental and a harmonic, and an amplitude equation with cubic nonlinearity is derived in the classical way. An objection to this methodology for the jet problem is that linear stability always gives a band of unstable waves which is unchanged as physical parameters are varied, in this case the capillary number. The evolution equation, then, is only valid for small enough times and in particular cannot describe pinching since that requires amplitude levels beyond the theory's range of validity. Chaudhary and Redekopp used their amplitude equations beyond their range of validity to produce pictures that qualitatively agree with experimental observations of breakup; there is no reason, however, to expect any quantitative agreement and in particular accurate solutions near breakup.

An improvement from weakly nonlinear theories is to allow the interfacial amplitude to be arbitrary but its wavelength to be long compared to the undisturbed jet radius. This is in the spirit of shallow water wave theories (see Whitham [47] for example), and through a systematic asymptotic expansion one-dimensional models of the Euler equations arise; the small parameter used is the ratio of the undisturbed jet radius to a typical perturbation wavelength. This was done by Ting and Keller [44], referred to as TK, who derive and study the leading order system. TK construct similarity solutions of their equations and use them to study the flow just beyond pinching by improving the original arguments of Taylor [43] and Keller [18]. A further improvement has been recently added by Keller, King and Ting [19] who solve the Euler equations for the flow in the attached fluid blob and match it to the slender filament which is a solution of the slender jet equations. It has been found out recently (see Papageorgiou [29], Papageorgiou and Orellana [30]) that the initial value problem based on the TK system terminates in an infinite slope singularity before the jet radius vanishes to form a pinch (see later also). It seems unlikely, therefore, that the leading order equations can describe pinching and keeping within the context of long-waves additional terms in the expansion need to be kept. Such models have been known for some years and are collectively called Cosserat models. A review can be found in Bogy [2], Meseguer [25] and

a more recent work with additional references is that of Garcia and Castellanos [14]. It appears that one of the original computations based on a one-dimensional model is that of Lee [22]; it was found that the Lee model supports pinching solutions but as our numerical studies indicate the jet develops a cusp near pinching - this in turn implies the violation of the slender jet assumption at the time of pinching and the full Euler equations need to be incorporated in an inner region. A weakly nonlinear version of the Cosserat model has been used by Schulkes [35] as a basis for a computational study. Schulkes [36] makes an evaluation of the weakly nonlinear model with the Lee model by solving the one-dimensional systems numerically; the local behavior very close to pinching was not studied, however.

Even though the one-dimensional models are useful and desirable, it appears that for inviscid jets at least, it may be necessary to relax the slenderness assumption and work with the full Euler equations. This is the axisymmetric extension of the work of Keller and Miksis [20] who compute the evolution of a break in a fluid sheet (the slender theory of this can be found in TK). A similarity solution of the Euler equations with all the terms balancing as a pinch forms, is possible then but has not been computed yet - see Papageorgiou [29]. Such solutions would be useful in comparisons with simulations based on the Euler equations. Such computations are usually based on boundary integral methods and have been performed by Mansour and Lundgren [24] for breakup of a liquid column and for related problems such as pendant drop bifurcations and contraction of liquid filaments by Schulkes [37], [38], [39]. A detailed quantitative comparison between computations and local similarity pinching solutions has not been carried out yet.

The difficulties encountered in inviscid one-dimensional models are removed when viscosity is added in the sense that the slenderness assumption is valid all the way to pinching governed by the leading order equations. Both Stokes and Navier-Stokes jets are considered. In the absence of inertia a one-dimensional model of the Stokes equations was first derived by Renardy [32] who also includes various viscoelastic models. Using the slender jet equations, Renardy proved that a Newtonian jet will break after a finite time given appropriate initial conditions. The solutions near the singular time are self-similar and have been given by Papageorgiou [28] who obtains an implicitly defined closed form solution with universal scaling exponents; in addition the scaling functions are universal to within a stretching factor that comes from initial conditions. All the theoretical results were confirmed by numerical solutions with different initial conditions. The jet shape is locally symmetric near the pinch point and the minimum jet radius goes to zero like $(t_s - t)^\beta$ with $\beta \approx 0.175$ and t_s the singular time which depends on initial conditions. Other forms of breakup similarity solutions are given by Renardy [33] and correspond to different initial conditions. In the study of Papageorgiou [28] the initial conditions are smooth.

Direct numerical simulations based on the Stokes equations and the boundary integral technique are usually carried out by inclusion of a surrounding fluid. In fact the single jet problem is usually computed by taking the appropriate viscosity ratio limit. Such computations have been developed by, for example, Stone and Leal [41] and Tjahjadi, Stone and Ottino [45]. An evaluation of the self-similar solutions of Renardy and Papageorgiou using the direct simulations remains to be carried out.

Inclusion of inertia into the Stokes theories enables construction of pinching solutions based on the Navier-Stokes equations. The analogous set of evolution equations was first obtained by Eggers and Dupont [13] who used local Taylor expansions assuming slenderness. An equivalent derivation has been given by Papageorgiou [28] using a slight modification of the systematic asymptotic expansion procedure applied to Stokes jets, by increasing the Reynolds number away from zero and scaling it with the expansion parameter. It should be noted that the model of Eggers and Dupont includes the complete curvature terms in the normal stress balance even though not all terms there are of the same asymptotic order. Eggers [11], [12], has computed the self-similar

solutions near breakup according to the one-dimensional model and provides strong numerical evidence that the scaling exponents and scaling functions are universal. In addition the breakup is non-symmetric in general if the initial conditions are also non-symmetric - this is in contrast to the Stokes models which produce locally symmetric pinching jet shapes even if the initial conditions are non-symmetric. It appears that the one-dimensional models do very well in describing the pinching dynamics and could be used in hybrid numerical methods to continue computations beyond a change in topology. It would be interesting to compare the theoretical predictions with direct numerical simulations of the Navier-Stokes equations. There have been some recent advances in this direction and we cite the work of Richards, Lenhoff and Beris [34], and a review can be found in Beris et al. [1].

In the theories described above the analytical approach is divided into two steps: First, a simplified set of one-dimensional PDE's is derived by assuming slenderness; second, these PDE's are analyzed for pinching self-similar solutions and determination of scaling exponents and functions. In solving initial value problems, then, the jet is assumed to be slender throughout the evolution. It is possible, however, that the evolution prior to pinching does not obey the slenderness criterion but only does so near pinching and locally near the pinch point. One can look for local solutions of the full equations of motion with a slenderness ratio which is time dependent and in fact approaches zero as the singular time is reached. The two steps are combined into one and the final result is a set of ODE's for the self-similar scaling functions; these are of course the same as the two step approach. This method avoids any problems with transient behavior of the evolution systems and gives a clearer structure of the singular solutions of the full equations. Such constructions starting from the Euler, Stokes and Navier-Stokes equations can be found in Papageorgiou [29] and is described later.

The structure of the article is as follows. Section 2 is devoted to the study of breakup according to the Euler equations. One-dimensional models are considered first and evidence is given suggesting the need of non-slender inner solutions; the equations governing such inner solutions are also derived and partly analyzed. Section 3 looks at Stokes jets and includes the analysis of pinching solutions both from the one-dimensional model as well as directly from the equations. Numerical solutions are presented that confirm the theoretical predictions. A modification of the expansion in Section 3 leads to jets with inertia and a model identical to that of Eggers [11]. We show how the universal scaling functions can be used to continue the dynamics beyond pinching. This is included in Section 4. Section 5 includes conclusions and thoughts on future work.

2 Inviscid jets governed by the Euler equations

Using a cylindrical coordinate system and looking at irrotational axisymmetric flows, the equations of motion can be written in terms of a velocity potential $\phi(t,r,z)$ where t is time, r is the radial and z the axial coordinate. The corresponding velocity field is $\mathbf{u} = (u,v,w) = \nabla\phi$. The governing equations and boundary conditions are

$$\phi_{rr} + \frac{1}{r}\phi_r + \phi_{zz} = 0. \tag{1}$$

On $r = S(t,z)$

$$\phi_r = S_t + \phi_z S_z, \tag{2}$$

$$\phi_t + \frac{1}{2}(\phi_r^2 + \phi_z^2) = -\left(\frac{1}{S} - S_{zz} + \frac{S_z^2 S_{zz}}{1+S_z^2}\right)(1+S_z^2)^{-1/2}. \tag{3}$$

In addition we require regularity of velocities at $r = 0$. The equations and boundary conditions have been non-dimensionalized using the undisturbed jet radius R as a length scale, the quantity $(\rho R^3/\sigma)^{1/2}$ as a time scale (this is the time scale of capillary instability), while the potential is scaled by $(R\sigma/\rho)^{1/2}$; ρ and σ denote fluid density and surface tension coefficient between the liquid and air. If initial and boundary conditions are prescribed (for instance periodic boundary conditions) the system (1)-(3) is closed and must be addressed numerically in general. In what follows we consider possible analytical developments.

2.1 Slender jet theory: One-dimensional models

Consider a small positive parameter ϵ which physically measures the ratio of a typical interfacial amplitude to a typical wavelength. The following change of variables gives the long wave equations to be studied,

$$\partial_r \to \partial_r, \qquad \partial_z \to \epsilon\partial_z, \qquad \partial_t \to \epsilon\partial_t, \qquad \phi \to \frac{1}{\epsilon}\phi,$$

which casts (1)-(3) into

$$\phi_{rr} + \frac{1}{r}\phi_r + \epsilon^2\phi_{zz}, \tag{4}$$

on $r = S(t,z)$

$$\phi_r = \epsilon^2(S_t + \phi_z S_z), \tag{5}$$

$$\phi_t + \frac{1}{2}\left(\frac{\phi_r^2}{\epsilon^2} + \phi_z^2\right) = -\left(\frac{1}{S} - \epsilon^2 S_{zz} + \frac{\epsilon^4 S_z^2 S_{zz}}{1+\epsilon^2 S_z^2}\right)(1+\epsilon^2 S_z^2)^{-1/2}. \tag{6}$$

An asymptotic expansion for ϕ proceeds in powers of ϵ^2

$$\phi = \phi_0 + \epsilon^2\phi_1 + \ldots,$$

and the leading order solutions follow from (4):

$$\phi_0 \equiv \phi_0(t,z), \qquad \phi_1 = -\frac{1}{4}r^2\phi_{0zz}. \tag{7}$$

Using these solutions into (5)-(6) yields the following system correct to $O(\epsilon^2)$:

$$S_t + \frac{1}{2}S\phi_{0zz} + S_z\phi_{0z} = 0, \tag{8}$$

$$\phi_{0t} + \frac{1}{2}\phi_{0z}^2 + \frac{1}{8}\epsilon^2 S^2(\phi_{0zz}^2 - 2\phi_{0z}\phi_{0zzz} - 2\phi_{0zzt}) = -\frac{1}{S} + \epsilon^2 S_{zz} + \epsilon^2\frac{S_z^2}{2S}. \tag{9}$$

Next, defining $W = \phi_{0z}$ and differentiating (9) by z we get the following system governing the evolution of the jet shape and the axial velocity:

$$(S^2)_t + (S^2W)_z = 0, \tag{10}$$

$$W_t + WW_z + \frac{1}{8}\epsilon^2\Big(S^2(W_z^2 - 2WW_{zz} - 2W_{zt})\Big)_z = \frac{S_z}{S^2} + \epsilon^2 S_{zzz} + \frac{1}{2}\epsilon^2\left(\frac{S_z^2}{S}\right)_z. \tag{11}$$

For a more detailed derivation as well as the inclusion of a surrounding fluid see Papageorgiou and Orellana (1995).

When $\epsilon = 0$ equations (10)-(11) are equivalent to the system studied by TK. It has been found by us, however, that this system terminates in "shock" finite time singularities and consequently the slender jet assumption is violated before the radius vanishes. The evidence is numerical by solution of the initial value problem on periodic domains using spectral methods, and also analytical by treating the system as a 2×2 system of conservation laws which becomes hyperbolic in the complex plane when the dependent and independent variables, but not time, are complexified. Riemann invariants are used to show that there are envelopes of characteristics which reach the real axis and thus a shock forms after a finite time. For small amplitude initial conditions the numerically computed singular times are in excellent agreement with the theoretical predictions. For full details of this analysis and the accompanying computations see Papageorgiou and Orellana (1995). Much of this theory stems from the pioneering work of Moore [26], [27] on singularity formation in vortex sheets and the subsequent work of Caflisch and Orellana [5], [6]. Also of interest is the related recent work of Caflisch et al. [4].

Since our interest is in drop formation we contemplate next regularizations of the TK equations as in (10) and (11). In particular we will present here the analysis of the Lee model which serves as a good illustrative starting point in the evaluation of one-dimensional inviscid models. We note that this model has been used by several investigators including Lee [22], Meseguer [25] and Schulkes [35], [36] - see Introduction also. The Lee model derives by dropping the ϵ^2 terms from the left hand side of (11) but keeping the full curvature terms on the right. The model considered here does not keep the full curvature terms but ignores the ϵ^2 terms on the left. Preliminary numerical results show that the retainment of the full curvature term has little effect on the final structure of the singularity. The model to be studied next, which is also known as a slice model, is

$$(S^2)_t + (S^2 W)_z = 0, \tag{12}$$

$$W_t + W W_z = \frac{S_z}{S^2} + \epsilon^2 S_{zzz} + \frac{1}{2}\epsilon^2 \left(\frac{S_z^2}{S} \right)_z . \tag{13}$$

We note that without loss of generality we can scale ϵ out of the problem by the transformations

$$S \to \frac{1}{\epsilon} S, \qquad W \to \sqrt{\epsilon} W, \qquad t \to \frac{1}{\sqrt{\epsilon}} t, \qquad z \to t.$$

Mathematically, these transformations do not alter the form of the singularities which we are analyzing.

2.2 Finite time singularities

Assuming that after a time t_s the jet radius vanishes at some position z_s, we look for solutions near this time and position, of the form

$$S(z,t) = \tau^{\alpha} h(\xi), \qquad W(z,t) = \tau^{\beta - 1} g(\xi), \qquad \xi = \frac{z - z_s}{\tau^{\beta}}, \tag{14}$$

where $\tau = t_s - t > 0$. We note that the scaling for W arises from a balance of terms, as $\tau \to 0$, in the mass balance equation (12). The value of α depends on which terms are in balance in the Bernoulli equation (13) near the singular time. A reasonable assumption would be to assume that all terms in (12) are in balance as $\tau \to 0$ which in turn fixes that $\alpha = \beta = 2/3$. Similarity solutions can then be constructed by study of the corresponding ODE's for the scaling functions. We have found, however, by numerical solution of the evolution equations (12) and (13) that the most likely scenario is one that has

$$\beta > \alpha. \tag{15}$$

Applying this inequality and an orders-of-magnitude argument to (13) it is found that the term S_z/S^2 on the right is negligible as $\tau \to 0$, and the balance gives

$$\alpha = 4\beta - 2. \tag{16}$$

Substitution of the ansatz (14) into the evolution equations along with the inequality (15) yields the following equations for the scaling functions

$$-4(2\beta - 1)h^2 + 2\beta\xi hh' + h^2g' + 2ghh' = 0, \tag{17}$$

$$(1-\beta)g + (\beta\xi + g)g' = h''' + \frac{1}{2}\left(\frac{h'^2}{h}\right)'. \tag{18}$$

The inequality (15) implies that as the jet radius vanishes the interface develops a cusp there and so the slender jet ansatz is violated. The situation is better than in the TK model, however, since that model does not support the vanishing of the jet radius before the long wave assumption is violated. It is routine to compute representative scaling functions - a four parameter family of similarity solutions is obtained by specification of $g(0), h(0), h'(0), h''(0)$ and integration to $\pm\infty$. A subset of this family has symmetry in h and anti-symmetry in g, which is a property of the equations. For this case, the asymptotic behavior at infinity is easily found to be

$$h(\xi) \sim A\xi^{4\beta-2}\beta, \qquad g(\xi) \sim \xi^{-\frac{1-\beta}{\beta}},$$

with A and B constants. Next order corrections can be calculated and decaying oscillations at infinity are found by application of a WKB method - see [30] for details. ¿From the numerical solution of the evolution equations (see next subsection) it is found that the most likely case is $\beta = 0.6$, $\alpha = 0.4$. These values imply $h \sim \xi^{2/3}$ and this power law was confirmed with solutions of (17)-(18) which give the exponent value to be 0.668. (The conditions for these solutions are $g(0) = 0$, $h(0) = 1$, $h'(0) = 0$, $h''(0) = 0.5$.)

2.3 Numerical solution of the evolution equations

Equations (12)-(13) were solved numerically using accurate pseudospectral methods (see also [30]); as explained earlier, we take $\epsilon = 1$. Periodic boundary conditions are imposed and in addition (this is not built into the numerical scheme) the symmetries of the equations are utilized by giving initial conditions $S(z,0) = S_0(z)$ and $W(z,0) = W_0(z)$ which are even and odd respectively about $z = \pi$ where the spatial domain is $[0, 2\pi]$. This implies that $S(z,t)$ and $W(z,t)$ remain even and odd respectively for subsequent times. The initial conditions used in the results that follow are

$$S_0(z) = a + a_1\cos(z), \qquad W_0(z) = -b\sin(z), \tag{19}$$

where $a > |a_1|$. The integrals $\int_0^{2\pi} W(z,t)dz$ and $\int_0^{2\pi} S^2(z,t)dz$ are conserved quantities and were used to monitor the accuracy of the computations.

The evolution of a typical run having $b = 0.1$, $a = 0.5$ and $a_1 = 0$ is shown in Figure 1. It is seen that drop formation appears after a finite time with the minimum jet radius going to zero at two symmetrically placed positions with the corresponding axial velocity blowing up there, as expected. (Fluid is ejected out of the drop which is forming.) The computations were stopped when (i) the minimum jet radius dropped below 0.01, (ii) the value of $\max|W|$ exceeded 20, or, (iii) the value of $\max|W_z|$ exceeded 100. Improvements can be made by inclusion of more modes but it is found that these criteria are sufficient to infer singular times and scaling laws, for example, described next.

2.4 Singular times and scaling laws

The time of the singularity is an unknown quantity and depends on the initial conditions. It is important to have a suitable method of obtaining an accurate estimate of this in order to use it in the estimation of scaling exponents. The following method appears to be the most suitable one and in particular it is insensitive to the type of ansatz we wish to evaluate. From the analysis presented earlier we expect that as a pinch forms the value of W_z blows up as τ^{-1} independently of the values of the exponents α and β. Letting $\max|W_z| = W_m(t)$ we have

$$\frac{1}{W_m(t)} \sim (t_s - t) \quad \text{as} \quad t \to t_s - . \tag{20}$$

Plots of $\frac{1}{W_m(t)}$ produced linear behavior by the end of the computation and a least squares fit of this linear part was used to extrapolate and estimate t_s. This procedure is depicted in Figure 2 which corresponds to initial conditions with $a = 0.5$, $a_1 = 0$ and $b = 0.05$. Singular times for different initial conditions with b varying were also computed.

With the singular times known we turn next to the estimation of the exponents α and β (see (14)). It is useful to define $S_{min}(t) = \min(S(z,t))$ and $W_{max}(t) = \max(W(z,t))$, noting that these are known from a given run. Plots of $\ln(S_{min})$ against $\ln(\tau)$ and $\ln(W_{max})$ against $\ln(\tau)$ should yield straight lines near the singular time (i.e., as $\tau \to 0$) with slopes equal to α and $\beta - 1$ respectively. Figures 3a-b depict such estimates for the representative case $b = 0.25$. Clearly $\alpha < \beta$ and so a cusp singularity is forming. As described earlier a balance of terms in the Bernoulli equation as $\tau \to 0$ yields the relationship (16) between α and β. It is important to test this balance for a range of initial conditions. Note that for the example of Figure 3, the estimated values of $4\beta - 2$ and α are 0.52 and 0.44 respectively and are fairly close given the sensitivity of the computations. A summary of results for various initial conditions is given in Table 1 below which contains estimates of t_s, α, β as well as $4\beta - 2$ which should be compared with the value of α as indicated by the balance (16).

b	.005	.01	.025	.05	.075	.1	.125	.15	.175	.2	.225	.25	.275	.3
t_s	5.89	5.10	4.05	3.25	2.73	2.29	1.94	1.66	1.44	1.25	1.08	.938	.810	.695
α	.47	.48	.47	.46	.46	.46	.49	.47	.47	.47	.45	.44	.43	.43
β	.61	.53	.61	.59	.59	.61	.64	.61	.6	.62	.6	.63	.56	.57
$4\beta - 2$	.44	.12	.44	.36	.36	.44	.56	.44	.4	.48	.4	.52	.24	.28

These results indicate strong evidence of cusp formation and they are consistent with the relationship (16).

Other features of the dynamics can be quantified using the model equations. For instance it has been shown that breakup according to the most amplified linear wave (this is an empirical engineering estimate) underestimates the singular time. More interestingly, the model predicts drop formation and can be used to compute the drop volume for different initial conditions. It has been found (for the symmetric initial conditions used here at least) that the drop volume roughly varies according to the estimate

$$V_{drop} = 0.51 \exp(-8.6b).$$

This is estimated from our computations and interpolation of the data.

2.5 Non-slender breakup

The cusp singularities at breakup violate the slender jet ansatz and an inner solution must be sought which does not assume scale disparity. Accordingly, the following transformations provide exact

similarity solutions of the Euler equations in the sense that all terms in the governing equations are in balance then (note that such an ansatz follows from a dimensional analysis also, as applied by Keller and Miksis [20] for the breakup of a fluid sheet).

$$(r,z) = \tau^{2/3}(y,\xi), \qquad S(z,t) = \tau^{2/3} f(\xi), \qquad \phi(r,z,t) = \tau^{1/3}\chi(y,\xi). \tag{21}$$

Substitution of (21) into the governing equations (1)-(3) yields the following problem to be solved:

$$\chi_{yy} + \frac{1}{y}\chi_y + \chi_{\xi\xi} = 0. \tag{22}$$

On $y = f(\xi)$,

$$\chi_y = \frac{2}{3}(\xi f' - f) + f'\chi_\xi, \tag{23}$$

$$\frac{1}{3}(2\xi\chi_\xi + 2f\chi_y - \chi) + \frac{1}{2}(\chi_y^2 + \chi_\xi^2) = -\left[\frac{1}{f} - f'' + \frac{f'^2 f''}{1+f'^2}\right](1+f'^2)^{-1/2}. \tag{24}$$

Note that equations (22)-(24) are the axially symmetric analogue of those used in [20].

3 Viscous jets

When viscosity is important the pertinent scales for capillary instability are σ/μ for velocities, σ/R for pressure and $\mu R/\sigma$ for time, where μ is the kinematic viscosity of the fluid. The non-dimensional form of the radially symmetric Navier-Stokes equations together with boundary conditions are:

$$R_e(u_t + uu_r + uw_z) = -p_r + \Delta u - \frac{u}{r^2}, \tag{25}$$

$$R_e(w_t + uw_r + ww_z) = -p_z + \Delta w, \tag{26}$$

$$u_r + \frac{u}{r} + w_z = 0, \tag{27}$$

where Δ denotes the Laplacian in cylindrical coordinates. On the interface $r = S(z,t)$:

$$(u_z + w_r)(1 - S_z^2) + 2u_r S_z - 2w_z S_z = 0, \tag{28}$$

$$p(1+S_z^2) - 2u_r - 2w_z S_z^2 + 2(u_z + w_r)S_z = -\left[\frac{S_{zz}}{\sqrt{1+S_z^2}} - \frac{\sqrt{1+S_z^2}}{S}\right], \tag{29}$$

$$u = S_t + wS_z. \tag{30}$$

In addition to the interfacial conditions (28)-(30), we require boundedness of solution at $r = 0$. The non-dimensional group $R_e = (\sigma\rho R/\mu^2)$ is the reciprocal of the capillary number, C_a.

In general a numerical solution of this system is required and possible approaches, when a surrounding fluid is present, are described elsewhere in [34] and also the article of Beris et al. in this volume. In what follows we use asymptotic methods to tackle the problem of jet pinching, viewing such an event as a finite time singularity of the PDEs. Such analyses are of value in evaluating direct numerical simulation and in the continuation of the dynamics beyond pinching by rational rather than ad hoc approaches.

3.1 Slender jet theory

The ideas follow those of the inviscid analysis where essentially we transform the governing equations according to $\partial/\partial z \rightarrow \epsilon\partial/\partial z$. In order to bring in unsteady and nonlinear terms into the leading order evolution the following ordering of R_e is required,

$$R_e = \epsilon^2\kappa, \qquad \kappa = O(1). \tag{31}$$

When $\kappa = 0$ we recover the slender jet equations for Stokes flow. An asymptotic solution is sought in powers of ϵ^2 as $\epsilon \rightarrow 0$ in the form

$$u(t,r,z) = u_0 + \epsilon^2 u_1 + \ldots, \tag{32}$$

$$w(t,r,z) = \frac{1}{\epsilon} w_0 + \epsilon w_1 + \ldots, \tag{33}$$

$$p(t,r,z) = p_0 + \epsilon^2 p_1 + \ldots, \tag{34}$$

$$S(t,z) = S_0 + \epsilon^2 S_1 + \ldots. \tag{35}$$

Substituting (31)-(35) into the governing equations (25)-(27) and collecting terms gives a series of simpler problems to solve. To leading order the axial momentum equation (26) and the continuity equation (27) provide the leading order flow field in terms of a single unknown function of z and t:

$$w_0 \equiv w_0(t,z), \qquad u_0 = -\frac{1}{2} r w_{0z}. \tag{36}$$

At the next order equation (26) gives

$$\kappa(w_{0t} + w_0 w_{0z}) = -p_{0z} + w_{1rr} + \frac{1}{r} w_{1r} + w_{0zz}, \tag{37}$$

while at leading order the radial momentum equation (25) brings in the radial variations in pressure:

$$p_{0r} = u_{0rr} + \frac{1}{r} u_{0r} - \frac{u_0}{r^2}. \tag{38}$$

Substitution of the solution for u_0 (36) into the equation for the leading order radial pressure gradient (38) shows that the latter is zero and so is independent of r. We write, then,

$$p_0 \equiv p_0(t,z).$$

Since the pressure does not vary radially, to leading order at least, it must be equal to its value just below the jet surface. The normal stress balance (29) allows its evaluation (using the leading order flow field already calculated):

$$p_0 = \frac{1}{S_0} - w_{0z}. \tag{39}$$

We have two unknowns, S_0 and w_0, and have yet to use the tangential stress balance (28) and the kinematic condition (29). A system of leading order evolution equations is found as follows: We first solve for the axial perturbation velocity w_1 from equation (37); this is easily done since the forcing terms involve w_0 and p_0 which are both independent of r. With w_1 at our disposal we can evaluate the two leading orders in the tangential stress balance equation (28). The leading order contribution is trivial ($w_{0r} = 0$) while the next order contribution gives a PDE involving w_0 and

S_0. Secondly, the kinematic condition is known to leading order since the flow field is also known to that order. The following coupled system of PDEs needs to be addressed, then:

$$\kappa(w_{0t} + w_0 w_{0z}) = \frac{3(S_0^2 w_{0z})_z}{S_0^2} - \left(\frac{1}{S_0}\right)_z, \tag{40}$$

$$S_{0t} + \frac{1}{2} S_0 w_{0z} + w_0 S_{0z} = 0. \tag{41}$$

The system (40)-(41) must be addressed numerically in general. We note that κ can be scaled out of the problem but is retained in order to clarify the Stokes limit considered next. A derivation and a numerical study of (40)-(41) was first carried out by Eggers and Dupont [13] using a different but related expansion scheme and additional work can be found in Eggers [11], [12], Papageorgiou [28], [29] and Renardy [32], [33]. The latter author considers inertialess flows. In what follows we consider the two distinct limits of Stokes flows (no inertia $\kappa = 0$) and flows with inertia.

4 The model equations for Stokes flows

With $\kappa = 0$ equation (40) can be integrated once to give

$$w_{0z} = \frac{1}{3}\left(\frac{\lambda(t)}{S_0^2} - \frac{1}{S_0}\right), \tag{42}$$

where the function $\lambda(t)$ represents the force in the jet (this force is independent of z since the flow is inertialess - see Renardy [32] and Papageorgiou [28]) and is to be found. If in addition we impose spatial periodicity, as will be done in the numerical experiments presented later, a further integration of (42) gives the dependence of the quasi-uniform force in terms of the jet shape,

$$\lambda(t) = \frac{\int_0^{2\pi} (1/S_0) dz}{\int_0^{2\pi} (1/S_0^2) dz}, \tag{43}$$

where, without loss of generality, the period has been normalized to 2π. This expression is useful in the numerical work given later.

4.1 Finite time singularities and self-similar solutions

Assume that the jet pinches after a finite time t_s. Then the minimum jet radius vanishes at $t = t_s$ at some axial position $z = z_s$. The objective is to obtain a description of the flow in the vicinity of this space-time singularity. Denoting $\tau = t_s - t$, we construct solutions in the limit $0 < \tau \ll 1$ near the position $z = z_s$, i.e. as $|z - z_s| \to 0$. Working with (40)-(41) and employing an order-of-magnitudes estimate (see Papageorgiou [28]) we may look for similarity solutions of the form

$$S_0(t,z) = \tau f(\xi), \quad w_0(t,z) = \tau^{\beta-1} g(\xi), \quad \xi = (z - z_s)^{\tau^\beta} \tag{44}$$

where $0 < \beta < 1$ and the scaling functions $f(\xi)$ and $g(\xi)$ are to be found. Substitution of (44) into (40) and (41) with $\kappa = 0$, yields the following set of nonlinear ODEs to solve on $\xi \in (-\infty, \infty)$:

$$\frac{d}{d\xi}(3f^2 g' + f) = 0, \tag{45}$$

$$(g + \beta\xi) f' + (\frac{1}{2} g' - 1) f = 0. \tag{46}$$

As before, equation (45) may be integrated once to obtain

$$g' = -\frac{1}{3f} + \frac{k}{f^2}, \tag{47}$$

where k is a constant of integration which is expressible in terms of f once we note that $g(\xi) \to 0$ as $|\xi| \to \infty$; integration of (47) gives

$$k = \frac{1}{3}\frac{\int_{-\infty}^{\infty}(1/f)d\xi}{\int_{-\infty}^{\infty}(1/f^2)d\xi}. \tag{48}$$

This expression for k can be used to obtain the form of $\lambda(t)$ as $t \to t_s$. Substitution of the similarity scalings (44) into (42) and integration of the resulting expression with respect to ξ using the decay of g at infinity, leads to

$$\lambda = 3k(t_s - t) \qquad \text{as} \quad \mathrm{t} \to \mathrm{t_s} - . \tag{49}$$

This assertion follows from the analysis but needs to be checked from a solution of the initial value problem for (40)-(41) for $\kappa = 0$.

4.2 Solution of the similarity equations

It is easy to establish the behavior of f and g for large $|\xi|$. This can be done by directly balancing terms in the ODEs or equivalently noting that the solutions at infinity be independent of t when written in terms of outer variables. Both approaches lead to

$$f(\xi) \sim |\xi|^{1/\beta}, \qquad g(\xi) \sim |\xi|^{-(1-\beta)/\beta} \qquad \text{as} \quad |\xi| \to \infty. \tag{50}$$

In terms of outer variables this asymptotic behavior provides matching conditions $S_0 \sim |z - z_s|^{1/\beta}$ and $w_0 \sim |z - z_s|^{-(1-\beta)/\beta}$ as $|z - z_s| \to 0$, the multiplicative constants coming from solution of the system (45) and (46). Since $g(\xi)$ tends to zero at infinity, there is a point, ξ_0 say, where $g(\xi_0) + \beta\xi_0 = 0$. Applying the transformations

$$f \to f, \qquad G(\eta) = g + \beta\xi_0, \qquad \eta = \xi - \xi_0,$$

shifts this point to the origin, $\eta = 0$, where $G(0) = 0$. The transformed equation (46) has a singular point at the origin which is removable if $G'(0) = 2$; the solutions are smooth, then. A local analysis of the equations for small η gives

$$f(\eta) = f_0 + \eta^2 f_2 + \eta^4 f_4 + \ldots, \qquad G(\eta) = 2\eta + \eta^3 g_3 + \ldots, \tag{51}$$

where we find

$$f_0 = \frac{1}{12(1+\beta)}, \qquad k = \frac{3+2\beta}{72(1+\beta)^2}, \tag{52}$$

with the remaining coefficients f_i and g_i, $i \geq 2$, expressible in terms of the single parameter f_2.

An implicitly defined closed form solution is available after elimination of G to obtain a second order ODE for f. This solution is (for details see Papageorgiou [28])

$$\begin{aligned} f &= \frac{1}{12(1+\beta)}\cos h^2(\theta), \\ \frac{1}{[12(1+\beta)]^\beta}\int_0^\theta \frac{(cosh^2\theta + 3 + 2\beta)^{\beta+1/2}}{\cosh\theta}d\theta &= \pm A\eta, \\ G(\eta) &= \int_{-\infty}^{\eta}\left(-\frac{1}{3f} + \frac{k}{f^2}\right)d\eta + \beta\xi_0, \end{aligned} \tag{53}$$

where

$$A = \frac{24}{(1+\beta)}\left(\frac{2+\beta}{6(1+\beta)}\right)^{\beta+1/2}\sqrt{f_2},$$

and $\pm$ corresponds to η positive and negative respectively. Evaluation of the solution $G(\eta)$ above, at $\pm\infty$ and use of the boundary conditions $G(-\infty) = G(\infty) = \beta\xi_0$ gives an expression for k identical to (48) noting the symmetry of f. The ratio is independent of f_2, so given β the solutions f and g are obtainable numerically. An eigenrelation must be satisfied, however, in order to obtain the correct β and the corresponding scaling functions. This relation arises from the two expressions of k given by (48) and (52) and reads

$$\frac{3+2\beta}{72(1+\beta)^2} = \frac{1}{3}\frac{\int_0^\infty (1/f)d\eta}{\int_0^\infty (1/f^2)d\eta}. \tag{54}$$

The computations give $\beta = 0.175$ correct to three decimals and this value appears to be unique. The effect of f_2 is in rescaling the axial coordinate as can be seen from the sample numerical results shown in Figure 4. The local theory provides similarity solutions which are unique to within a linear scaling transformation. The theory is a formal one and numerical solutions of the initial value problem are desirable to confirm the local theory. This is done next.

4.3 Numerical solutions of the initial value problem

The numerical methods employed to solve (40) and (41) for $\kappa = 0$ are described in Papageorgiou [28]. A pseudo-spectral method is used with axial periodicity; the boundary conditions are insensitive to the terminal state solutions since the latter are indeed of the local form given in the previous subsection. To fix matters we consider periodic solutions on $[0, 2\pi]$; the equations preserve symmetry and anti-symmetry respectively for S_0 and w_0 about $z = \pi$, and in the first set of numerical results we report on such parity solutions. The following initial conditions are used:

$$S_0(0, z) = a + b\cos(z), \tag{55}$$

where $a, b > 0$ and $a > b$. This means that there is a minimum in the jet shape at $z = \pi$ and due to symmetry the jet will first pinch there. In addition to S_0 and w_0 we also monitor the evolution of $\lambda(t)$ and the minimum jet radius denoted by $S_{min}(t)$. A typical run having $a = 0.5$ and $b = 0.1$ is given in Figure 5 which shows evolution of the jet shape and the corresponding axial velocity at different times up to $t = 6.5$. A cross-section of the jet is shown at the later time $t = 6.6$ in Figure 6; the Figure also shows the evolution of the maximum value of S_{0z} and confirms the validity of the slender jet assumption. Note that the singular time (see below for its estimation) is $t_s = 6.64$ and the minimum jet radius at $t = 6.6$ is 0.0028.

According to the predictions of the local theory, as the singular time is approached the following forms are attained by $S_{min}(t)$ and $\lambda(t)$:

$$S_{min}(t) \sim \frac{1}{12(1+\beta)}(t_s - t), \qquad \lambda(t) \sim \frac{3+2\beta}{24(1+\beta)^2}(t_s - t), \tag{56}$$

where $\beta = 0.175$. Considering either of these two expressions, then, we can estimate the singular time t_s since the behavior is linear near the singular time. This procedure is illustrated in Figure 7 using data from the previous run. The Figure shows the evolution of $S_{min}(t)$ and an enlargement of the later stages of the evolution together with the least squares linear extrapolation used in estimating t_s. This is how the value $t_s = 6.64$ was found. It is worth noting that the variation

of $S_{min}(t)$ is linear long before the singular time, i.e., the asymptotic behavior predicted by (56) for small $t_s - t$ is valid for most of the computational time - in fact from approximately $t = 2$ to $t = t_s$. Similar findings hold for a parallel analysis of the data from the $\lambda(t)$ evolution (see [28]). A further confirmation of the wide validity of the asymptotic solutions and the universal exponents, is given in Figure 8 which depicts the computed and theoretical evolutions of $S_{min}(t)$ and $\lambda(t)$; this is possible once t_s has been estimated and for the theoretical curves we use the results (56). Again agreement is seen to be excellent with the similarity solutions valid significantly before breakup.

The corresponding scaling functions are computed as follows: Knowledge of the singular time t_s, and hence $\tau = t_s - t$, allows the computation of the similarity independent variable ξ as the computation proceeds - this is given by $(z - \pi)/\tau^\beta$ for the run described earlier. The corresponding computed solutions at that particular time, $S_0(t, z)$ and $w_0(t, z)$, are next used together with the similarity ansatz (44) to construct the functions $f(\xi)$ and $g(\xi)$. The dependence of these functions on τ disappears as $\tau \to 0$ and this expectation is fully supported in the sample numerical results of Figure 9 which shows the corresponding $f(\xi)$ and $g(\xi)$ for different times approaching t_s.

Having established the universal predictions of the similarity theory for solutions containing special symmetry, we next consider breakup from more general initial conditions. In particular we report on a run having

$$S_0(0, z) = 0.5 + 0.1(\sin x + \cos x).$$

The evolution of S_0 and w_0 is given in Figure 10. The jet is breaking at a position $z = z_s(t)$ to the right of $z = \pi$. An estimate of the singular time can be made as in the symmetric case (the similarity theory is a local one) and the evolution of $S_{min}(t)$ and $\lambda(t)$ together with the theoretical predictions are shown in Figure 11. Again agreement is excellent. We also note that the breakup time is smaller. The theory presented in the previous subsection predicts scaling functions $f(\xi)$ and $g(\xi)$ which are even and odd respectively about $\xi = 0$. This prediction has been confirmed for this nonsymmetric run as follows: Take the last computed profiles S_0 and w_0. From the S_0 profile locate the point where the minimum is attained and call this z_0. Then S_0 is expected to be symmetric about $z = z_0$ and w_0 anti-symmetric. This is presented graphically in Figure 12 for S_0 and w_0 respectively. The Figure for S_0 was obtained by reflecting the solution for $z < z_0$ about $z = z_0$ and plotting it along with the solution for $z > z_0$, while that for w_0 is obtained by reflecting the solution about $z = z_0$, taking its negative, and plotting it together with the solution for $z > z_0$. Solid lines represent $z > z_0$ and the open circles correspond to reflected data. The two data sets are indistinguishable providing strong evidence for the local symmetry properties predicted by the similarity theory.

4.4 Universal scaling functions

In the previous subsections we established a way of (i) estimating the singular time t_s, (ii) using this estimate and numerical solutions near breakup to construct the scaling functions given by (44). In this section we consider the scaling functions for different initial conditions. Since breakup is locally symmetric we consider a one-parameter family of symmetric initial conditions of the form:

$$S_0(0, z) = 0.5 + b \cos z,$$

Runs with $b = 0.005, 0.01, 0.02, 0.03, 0.05, 0.1, 0.2, 0.3$ are reported. Figure 13 shows the evolution of $S_{min}(t)$ for the different values of b labeled on the Figure. In addition the asymptotic behavior of S_{min} near the singular time is superimposed for each run; the slopes of the curves are predicted by the theory to be $-1/12(1 + \beta)$ irrespective of initial conditions, and this is supported by the

results. Another interpretation of the equal slopes is that the $f(\xi)$ scaling functions satisfy $f(0) = 1/12(1+\beta)$ for the different values of b.

A more detailed study of the scaling functions is considered next. Using the methods of Section 4.3, scaling functions were constructed for different values of b. Representative results for $f(\xi)$ are shown in Figure 14a for b (denoted by ep in the Figure) equal to $0.005, 0.1, 0.2, 0.3$. The scaling functions coincide at $\xi = 0$; according to the theory of Section 4.2 and in particular the solutions (53), the only difference between scaling functions is in a re-scaling of the axial coordinate brought about by the presence of the constant f_2 which depends on the initial conditions. This is illustrated numerically from the data of Figure 14a as follows: Consider the run with $b = 0.1$ as a reference run and call the emerging scaling function $f_0(\eta)$. Then, according to the theory, there exists a positive number $c(b)$ such that the transformation $\eta \to c\eta$ maps the scaling function $f(\xi; b)$ into $f_0(\xi)$. The value of c can be obtained by consideration of a fixed interfacial height, h say, and is equal to the ratio η_0/η_i where $f_0(\eta_0) = f_i(\eta_i) = h$ with i corresponding to the different initial conditions. The c found from mapping a single point onto the curve $f_0(\eta)$ will map the whole curve onto $f_0(\eta)$, if the theory and the numerics coincide, and the procedure outlined has the dual purpose of (i) making a strong global validation of the similarity solutions, (ii) constructing "universal" scaling functions, noting that these are so to within a linear axial transformation. The results of this procedure are given in Figure 14b from which it is seen that all curves do collapse into the single $f_0(\eta)$ curve, in complete accord with the theory.

4.5 Pinching solutions of the Stokes equations

The Stokes equations for axially symmetric liquid threads are given by (25)-(27) with $R_e = 0$ and the same boundary conditions (28)-(30). Here we show how the two step procedure outlined above, that is the derivation of longwave equations followed by construction of pinching solutions, can be combined into one by essentially allowing the small parameter ϵ introduced into the longwave models, to become time dependent. Using the notation introduced earlier, we generalize the breakup by looking at solutions of the Stokes equations near the singular time, i.e., as $\tau \to 0$, of the form

$$r = \tau^\alpha y, \qquad z = \tau^\beta \xi, \qquad S = \tau^\alpha f(\xi),$$
$$w = \tau^\gamma W(t,y,\xi), \qquad u = \tau^{\gamma+\alpha-\beta} U(t,y,\xi), \qquad p = \tau^{-\alpha} P(t,y,\xi), \tag{57}$$

where without loss of generality we take the breaking point to be at $z = 0$. Note that the form of u follows from the continuity equation once w is assumed. We make the assumption that $\alpha > \beta$ which implies a slender geometry which is enhanced as the breaking time is approached; slenderness is not assumed throughout the evolution, then, but only near the pinch time. The quantity $\tau^{2\alpha-2\beta}$ is a small parameter, then, which appears naturally in the Stokes equations (in the biharmonic operator for the streamfunction, for instance). The following Taylor expansions are appropriate then,

$$\begin{aligned} w &= \tau^\gamma (g(\xi) + \tau^{2\alpha-2\beta} W_1 + \ldots), \\ u &= \tau^{\gamma+\alpha-\beta}(-\frac{1}{2} y g' + \tau^{2\alpha-2\beta} U_1 + \ldots), \\ P &= P_0(y,\xi) + \tau^{2\alpha-2\beta} P_1(y,\xi) + \ldots, \end{aligned} \tag{58}$$

which on substitution into the axial momentum equation (26) and balance of terms yields,

$$\gamma = \beta - \alpha, \qquad W_{1y} = \frac{1}{2} y (P_{0\xi} - g'').$$

This in turn leads to the expression for U_1 from the continuity equation and the result $P_y = 0$. Use of these results into the tangential and normal stress balance equations (28)-(29) gives at $O(\tau^{-\beta})$ and $O(\tau^{-\alpha})$ respectively, on $y = f(\xi)$:

$$(f^3 g')' = \frac{1}{2} f^3 P0', \qquad P_0(\xi) = -g' + \frac{1}{f},$$

and on integration with respect to ξ it yields

$$g' = -\frac{1}{3f} + \frac{k}{f^2}, \tag{59}$$

with k a constant. A leading order balance in the kinematic condition (30) gives the second equation

$$\alpha = 1, \qquad (g + \beta\xi) f' + (\frac{1}{2} g' - 1) f = 0. \tag{60}$$

To leading order, then, the equations for the scaling functions (59) and (60) are identical to those found in Section 4.1 and solution proceeds as before.

4.6 Validity of the similarity equations

As the jet pinches, the following velocity field is found,

$$w = \tau^{\beta-1} g(\xi) + \tau^{1-\beta} W_1 + \ldots, \qquad u = -\frac{1}{2} y g' + \tau^{2-2\beta} U_1 + \ldots. \tag{61}$$

The leading order axial velocity becomes infinite as $\tau \to 0+$ and since we are working within the context of the Stokes equations we need to check the effect of neglected inertial terms in the Navier-Stokes equations. More details may be found in Papageorgiou [28], [29]; briefly, it is found that the radial momentum equation approximation remains consistent as $\tau \to 0$; using the solutions (61) into the Navier-Stokes system shows that in deriving these solutions we keep terms of $O(\tau^{-1-\beta})$ while neglecting unsteady and nonlinear terms of $O(\tau^{\beta-2})$. Consistency of the Stokes solutions all the way to pinching, is possible then if the neglected Navier-Stokes terms remain asymptotically smaller as $\tau \to 0$. This requires $\beta - 2 \leq -1 - \beta$, or, $\beta \geq 1/2$ (equality brings in unsteady and nonlinear terms - see below). It can be concluded, therefore, that the similarity solutions for Stokes jets which were found analytically and confirmed numerically, break down as the jet pinches and unsteady and inertial terms enter then. For high viscosity fluids one can expect the Stokes solutions to be operational for part of the evolution. It is particularly interesting to note that our analysis indicates that numerical algorithms based on the Stokes equations, as in the boundary integral method for example, need to be interpreted with care as the jet pinches. Our analysis quantifies exactly how such Stokes solutions may break down and in what follows we present the evolution that enters at that stage.

5 Jet breakup for Navier-Stokes flows

In this Section we will show how the breakup for Stokes jets needs to be modified in order to get a consistent solution. This is done in two ways: First we follow the analysis of Section 4.6. A system of similarity equations is found for the scaling functions. We also consider pinching according to the model equations of Section 3.1 with $\kappa \neq 0$, and show that an identical system emerges. Finally we use these solutions to show how they can be used to continue the flow just beyond pinching by means of rational methods which obey the underlying physical principles, rather than introducing ad hoc regularizations as has been done by other authors.

5.1 Pinching solutions of the Navier-Stokes equations

Guided by the estimates of the various terms as the Stokes jet pinches (see Section 4.6) we take $\beta = 1/2$ and look for terminal states of the Navier-Stokes equations of the following form:

$$w = \tau^{-1/2} W_0(\xi) + \tau^{1/2} W_1(y,\xi) + \ldots, \quad u = U_0(y,\xi) + \tau U_1(y,\xi) + \ldots,$$
$$p = \tau^{-1} P(y,\xi) + \ldots, \quad S(t,z) = \tau f(\xi), \tag{62}$$
$$r = \tau y, \quad z = \tau^{1/2}\xi, \tag{63}$$

where as before we take $\tau = t_s - t$ with t_s the singular time and we assume, without loss of generality, that pinching occurs first at $z = 0$. The functions W_i, U_i, P are to be found. Substitution into the Navier-Stokes equations (25)-(26) gives to leading order,

$$P_y = 0, \tag{64}$$
$$R_e \left(\frac{1}{2}(W_0 + \xi W_0^\xi) + W_0 W_0^\xi \right) = -P' + W_{1yy} + \frac{1}{y} W_{1y}, \tag{65}$$

with primes denoting ξ-derivatives. The solution for W_1 is

$$W_1 = \frac{1}{4} y^2 \frac{d}{d\xi} \left(P - W_0' + \frac{1}{2} R_e (\xi W_0 + W_0^2) \right) + A(\xi), \tag{66}$$

with $A(\xi)$ some function of ξ; a solution for U_1 follows from the continuity equation (27). A coupled system of equations for W_0 and f is found as follows: (i) evaluation of P from the leading order contributions to the normal stress balance (29) and insertion into (66) to give W_{1y} in terms of desired functions, (ii) substitution of W_1 into the leading order contribution to the tangential stress balance equation (28) to yield one equation, (iii) evaluation of the leading terms of the kinematic equation (30) to give a second equation. The two equations are nonlinear ODEs and describe the similarity solutions within the pinch region. The equations read:

$$3W_0'' + \frac{f'}{f^2} + 6\frac{W_0' f'}{f} = R_e \left(\frac{1}{2}(W_0 + \xi W_0') + W_0 W_0' \right), \tag{67}$$
$$(W_0 + \frac{1}{2}\xi) f' - (1 - \frac{1}{2} W_0') f = 0. \tag{68}$$

These equations are identical to those first derived and solved by Eggers [11], [12] by analysis of the model one-dimensional PDEs as briefly described next.

5.2 Pinching solutions of the one-dimensional model equations

The equations to be considered are the model system (40) and (41). Using the notation and methodology of previous Sections we look for pinching self-similar solutions in the form

$$S_0(t,z) = \tau f(\xi), \quad w_0(t,z) = \tau^{-1/2} g(\xi), \quad z = \tau^{1/2}\xi. \tag{69}$$

Substitution of (69) into (40) and (41) keeps all terms in the equations of the same order in τ and yields exactly equations (67) and (68) where R_e is now replaced by κ; as mentioned earlier the constant κ may be scaled out of the problem to arrive at exactly the system studied by Eggers [11], [12].

Numerical solutions of the initial value problem according to the model system (40) and (41) were first given by Eggers and Dupont [13] and also by Eggers [11]. It is found that as pinching is approached, general non-parity initial conditions evolve into universal scaling functions which are

not symmetric in the jet shape, for instance. Solution of the similarity equations (67) and (68) were obtained by Eggers [11], [12] by use of a shooting method.

In our analysis of the dynamics beyond pinching, it is necessary to know the behavior of the scaling functions away from the pinch point, that is as the local inner solution is matched to the outer quasi-static solution. It is easily established that as $|\xi| \to \infty$ we have

$$f(\xi) \sim \xi^2, \qquad W_0(\xi) \sim \xi^{-1}.$$

More precisely, there are universal constants $b_1^{\pm}$ and $b_2^{\pm}$ such that

$$f(\xi) \sim b_1^{\pm}\xi^2, \qquad W_0(\xi) \sim b_2^{\pm}\xi^{-1} \quad \text{as } \xi \to \pm\infty. \tag{70}$$

Numerical computation (see [12]) gives these constants to be

$$b_1^+ = 4.635, \quad b_1^- = 6.074 \times 10^{-4}, \qquad b_2^+ = 0.0723, \quad b_2^- = 57.043.$$

Note that these forms at infinity imply that the jet shape is locally parabolic as a pinch forms, unlike the corresponding shapes for Stokes jets.

5.3 Dynamics beyond pinching

In this Section we follow the analysis of Papageorgiou [29] to show how the universal scaling functions described above can be used as the correct initial conditions for the flow just after the change of topology in order to obtain a theoretical description of the dynamics for small times just after pinching. The equivalent analysis for Stokes jets using the scaling functions of Section 4.2 can be found in [29].

The ideas used here are the viscous flow analogues of the methods originally developed by Taylor [43], Keller [18], Ting and Keller [44] and more recently Keller, King and Ting [19]. The solutions given in previous Sections describe the flow up to the time of breaking. Beyond this time the jet separates and the two ends accelerate away from the breaking point. Assuming that the jet ends at some axial position $X(t)$ and that a fluid blob of mass $M(t)$ is attached to that end, it is suggested that a fairly complete and rational picture of the dynamics beyond pinching is possible if one can solve for $X(t)$ and $M(t)$, for small times at least. These small time solutions (given below) are useful in initializing a direct numerical simulation correctly. We note that for the viscous case the exponents of the scaling functions are fixed and so the dynamics described below are universal. This is in contrast to the analysis of [44] where an exponent has to be chosen with different dynamics resulting. In addition this theory is rational in the sense that no ad hoc regularizations are made that can allow the jet to pinch and form fluid blobs even though the equations describing such motions are slender jet equations (see [12] for an ad hoc regularization). Instead we proceed by using momentum and mass balance arguments to obtain the evolution of $X(t)$ and $M(t)$ and use the correct initial conditions at $t = 0+$.

The first equation comes from a mass balance of the fluid inside the blob. Define $M(t)$ to be the blob mass and $X(t)$ to be the axial distance from the breaking point where the blob is attached to the slender jet. The jet radius at the point of attachment is $S(X(t), t)$ and W is the axial velocity there. All quantities are dimensional at this stage. The mass balance of fluid entering the blob through the attachment region is

$$\frac{dM}{dt} = \pi\rho S^2 \left(\frac{dX}{dt} - W\right). \tag{71}$$

Next consider balance of momentum using dimensional variables. The forces acting on the blob at $z = X(t)$ are due to viscous stresses and the pull due to surface tension. Denote the axial

component of the viscous stress by T_{zz} and the radial component by T_{rr}, then the total force acting on the cross-section at $X(t)$ is

$$F = \pi S^2(T_{zz} - p) + 2\pi\sigma S,$$

which on use of the normal stress balance equation (for slender jets)

$$p = T_{rr} + \frac{\sigma}{S},$$

becomes

$$F = \pi S^2(T_{zz} - T_{rr}) + \pi\sigma S = 3\pi\mu S^2 W_z + \pi\sigma S. \tag{72}$$

Note that for Stokes jets F_z is zero since Stokes flows do not possess inertia; this is recognized to be equation (40) with $\kappa = 0$ (see [32] also). With inertia present, however, a balance of momentum of the fluid blob is found using (72):

$$\frac{d}{dt}\left(M\frac{dX}{dt}\right) = 3\pi\mu S^2 W_z + \pi S + W\frac{dM}{dt}. \tag{73}$$

On use of the capillary scales of Section 3 the dimensionless forms of equations (71) and (73) are found to be

$$\frac{dM}{dt} = \pi S^2\left(\frac{dX}{dt} - W\right), \tag{74}$$

$$R_e\frac{d}{dt}\left(M\frac{dX}{dt}\right) = 3\pi S^2 W_z + \pi S + R_e W\frac{dM}{dt}, \tag{75}$$

where the same symbols are used in denoting dimensionless variables. Note also that the inviscid system studied by Ting and Keller [44], has the viscous term $3\pi S^2 W_z$ term missing from (75).

Equations (74) and (75) are to be solved subject to initial conditions, at $t = 0$ say, which are given by the terminal similarity states described in earlier Sections. In coupling the flow into the dynamics of the fluid blob, we require the behavior of the solutions for small but *positive* time. The Navier-Stokes were considered in Section 5 as the singular time was approached from below. The similarity equations just beyond pinching (assumed without loss of generality to occur at $t = 0$), in regions where the jet is slender at least, are obtained for $0 < t << 1$ by the ansatz (62) with $t > 0$ replacing τ; time derivatives are different now and following the same procedure the following equations need to be solved for the scaling functions f and g:

$$3W_0'' + \frac{f'}{f^2} + 6\frac{W_0' f'}{f} = -\frac{1}{2}(W_0 + \xi W_0') + W_0 W_0', \tag{76}$$

$$(W_0 - \frac{1}{2}\xi)f' + (1 + \frac{1}{2}W_0') = 0, \tag{77}$$

where $R_e = 1$, since it can be scaled out of the problem. In Section 5 we described the universal solution as the jet breaks; in particular, then, equations (76) and (77) must be solved subject to the conditions at infinity given by (70). For instance, choosing to follow the dynamics of the rightmost fluid blob, we take the conditions for large positive ξ provided by (70). These conditions are sufficient to determine unique scaling functions for smaller ξ by integrating inwards from infinity. The computation can be valid only as far as the point where the fluid blob begins, i.e., at $z = X(t)$ (the slender jet ansatz breaks down otherwise). Clearly then, we need to solve for $X(t)$ in order to find the appropriate scaling functions which in turn provide the evolution of $M(t)$.

Following Ting and Keller [44] we look for solutions of equations (74) and (75) for small t as follows:

$$X(t) = X_0 t^{1/2}, \quad S(t, X_0) = t f(X_0), \quad W(t, X_0) = t^{-1/2} W_0(X_0).$$

Substitution into (74)-(75) gives

$$M(t) = \frac{2}{5}\pi f^2(X_0)\left(\frac{1}{2}X_0 - W_0(X_0)\right)t^{5/2}, \tag{78}$$

$$\left(\frac{2}{5}X_0 - W_0(X_0)\right)\left(\frac{1}{2}X_0 - W_0(X_0)\right) f(X_0) - 3f(X_0)W_0'(X_0) = 1. \tag{79}$$

Note that equation (79) provides a condition that determines X_0. Numerically this is done as follows: Starting at large positive ξ and using the appropriate universal asymptotic forms (70) there, we integrate the system (76) and (77) inwards until the first point is found where equation (79) is satisfied. The numerical value found from the computations is $X_0 = 0.91$ correct to two decimals. With X_0 known (as well as the scaling functions there), we use (78) to compute the mass $M(t)$ at different times.

A schematic of the jet shapes, for instance, as time increases can be constructed as follows: We chose four different times $t = 0.0001 - 0.0004$. X_0 is computed as described above and so are $M(t)$ and $X(t) = X_0 t^{1/2}$. The point $X(t)$ marks the end of the slender part of the jet and the beginning of the fluid blob. We picture the jet shape by distributing the mass $M(t)$ over a sphere in order to compute its radius. Results of such calculations are given in [29]. We note that to within our treatment of the blob shape, the results are based on variables which are universal and so the small time solutions provide rational initial conditions for jet dynamics beyond breakup.

6 Conclusions

We have considered the breakup of liquid jets under the action of capillary instability. The phenomenon of drop formation which precedes the topological change in the shape has been analyzed by construction of local self-similar solutions for both viscous and inviscid jets. It has been demonstrated that viscous jets admit slender breakup and unique scaling exponents and functions. One-dimensional models based on a slender jet ansatz have also been solved numerically by specification of arbitrary smooth initial conditions, and exhibited to support the theoretical self-similar predictions. Leading order 1-D models are sufficient when viscosity is present, but higher order terms in the expansion must be incorporated into the evolution equations for inviscid flows. Such reduced models have also been analyzed for self-similar solutions as well as by numerical simulations, and the results indicate drop formation with a locally cusp-like behavior. The system governing the dynamics on the short scale that removes the cusp singularity is also given.

References

[1] Beris, A.N., Richards, J.R. and Lenhoff, A.M., "VOF/CSF methods applied to the liquid-liquid jet breakup and drop dynamics", Advances in Multi-Fluid Flows, Proceedings of the AMS-IMS-SIAM Joint Summer Research Conference on Multi-Fluid Flows and Interfacial Instabilities, (1995).

[2] Bogy, D.B., "Drop formation in a circular liquid jet," Ann. Rev. Fluid. Mech. **11**, 207 (1979).

[3] Brenner, M.P., Shi, X.D. and Nagel, S.R., "Iterated instabilities during droplet fission," Phys. Rev. Lett. **73**, 3391 (1994).

[4] Caflisch, R.E., Ercolani, N., Hou, T.Y. and Landis, Y., "Multi-valued solutions and branch point singularities for nonlinear hyperbolic or elliptic systems," Communications on Pure and Applied Mathematics Vol. XLVI, 453 (1993).

[5] Caflisch, R.E. and Orellana, O., "Long time existence for a slightly perturbed vortex sheet," Communications on Pure and Applied Mathematics Vol. XXXIX, 807 (1986).

[6] Caflisch, R.E. and Orellana, O., "Singular solutions and ill-posedness for the evolution of vortex sheets," SIAM J. Math. Anal. **20** No. 2, 293 (1989).

[7] Chaudhary, K.C. and Maxworthy, T., "The nonlinear capillary instability of a liquid jet. Part 2. Experiments on jet behavior before droplet formation," J. Fluid Mech. **96**, 275 (1980).

[8] Chaudhary, K.C. and Maxworthy, T., "The nonlinear capillary instability of a liquid jet. Part 3. Experiments on satellite drop formation and control," J. Fluid Mech. **96**, 287 (1980).

[9] Chaudhary, K.C. and Redekopp, L.G., "The nonlinear capillary instability of a liquid jet. Part 1. Theory," J. Fluid Mech. **96**, 257 (1980).

[10] Donelly, R.J. and Glaberson, W., "Experiments on the capillary instability of a liquid jet," Proc. R. Soc. London Ser. A **290**, 547 (1966).

[11] Eggers, J., "Universal pinching of 3D axisymmetric free-surface flow," Phys. Rev. Lett. **71**, 3458 (1993).

[12] Eggers, J., "Theory of drop formation," Phys. Fluids **7**(5), 941 (1995).

[13] Eggers, J. and Dupont, T.F., "Drop formation in a one-dimensional approximation of the Navier-Stokes equation," J. Fluid Mech. **262**, 205 (1994).

[14] García, F.J. and Castellanos, A., "One-dimensional models for slender axisymmetric viscous liquid jets," Phys. Fluids **6**, 2676 (1994).

[15] Goedde, E.F. and Yuen, M.C., "Experiments on liquid jet instability," J. Fluid Mech. **40**, 495 (1970).

[16] Hauser, E.A., Edgerton, H.E., Holt, B.M. and Cox, J.T., "The application of the high-speed motion picture camera to research the surface tension of liquids," J. Phys. Chem. **40**, 973 (1936).

[17] Lord Rayleigh, "On the stability of liquid jets," Proc. London Math. Soc. **10**, 4 (1878).

[18] Keller, J.B., "Breaking of liquid films and threads," Phys. Fluids **26**, 3451 (1983).

[19] Keller, J.B., King, A. and Ting, L., "Blob formation," Phys. Fluids **7**(1), 226 (1995).

[20] Keller, J.B. and Miksis, M.J., "Surface tension driven flows," SIAM J. Appl. Math. **43** No. 2, 268 (1983).

[21] Lafrance, P., "Nonlinear breakup of a laminar liquid jet," Phys. Fluids **18**(4), 428 (1975).

[22] Lee, H.C., "Drop formation in a liquid jet," IBM J. Res. Dev. **18**, 364 (1974).

[23] Lord Rayleigh, "On the stability of a cylinder of viscous liquid under capillary force," *Scientific Papers* (Cambridge University Press, Cambridge, 1902), Vol. 3, pp. 585-593 [also see Phil. Mag. **34**, 145 (1892)].

[24] Mansour, N. and Lundgren, T.S., "Satellite formation in capillary jet breakup," Phys. Fluids **2**(7), 1141 (1990).

[25] Meseguer, J., "The breaking of axisymmetric slender liquid bridges," J. Fluid Mech. **130**, 123 (1983).

[26] Moore, D.W., "The spontaneous appearance of a singularity in the shape of an evolving vortex sheet," Proc. R. Soc. London Ser. A **365**, 105 (1979).

[27] Moore, D.W., "Numerical and analytical aspects of Helmholtz instability," in Theoretical and Applied Mechanics, Proc. XVI ICTAM, eds. Niordson and Olhoff, North-Holland, pp. 263-274 (1984).

[28] Papageorgiou, D.T., "On the breakup of viscous liquid threads," Phys. Fluids **7**(7), 1529 (1995).

[29] Papageorgiou, D.T., "Analytical description of the breakup of liquid jets," J. Fluid Mech. **301**, 109 (1995).

[30] Papageorgiou, D.T. and Orellana, O., "Study of cylindrical jet breakup using one-dimensional approximations of the Euler equations," submitted to SIAM J. Appl. Math. [also CAMS Research Report 052].

[31] Peregrine, D.H., Shoker, G. and Symon, A., "The bifurcation of liquid bridges," J. Fluid Mech. **212**, 25 (1990).

[32] Renardy, M., "Some comments on the surface tension driven breakup (or lack of it) of viscoelastic jets," J. Non-Newtonian Fluid Mech. **51**, 97 (1994).

[33] Renardy, M., "A numerical study of the asymptotic evolution of Newtonian and viscoelastic jets," J. Non-Newtonian Fluid Mech., submitted, (1995).

[34] Richards, J.R., Lenhoff, A.M. and Beris, A.N., "Dynamic breakup of liquid-liquid jets," Phys. Fluids **6**, 2640 (1994).

[35] Schulkes, R.M.S.M., "Dynamics of liquid jets revisited," J. Fluid Mech. **250**, 635 (1993).

[36] Schulkes, R.M.S.M., "Nonlinear dynamics of liquid columns: A comparative study," Phys. Fluids A **5**(9), 2121 (1993).

[37] Schulkes, R.M.S.M., "The evolution of capillary fountains," J. Fluid Mech. **261**, 223 (1994).

[38] Schulkes, R.M.S.M., "The evolution and bifurcation of a pendant drop," J. Fluid Mech. **278**, 83 (1994).

[39] Schulkes, R.M.S.M., "The contraction of liquid filaments," J. Fluid Mech., submitted (1995).

[40] Shi, X.D., Brenner, M.P. and Nagel, S.R., "A cascade structure in a drop falling from a faucet," Science **265**, 157 (1994).

[41] Stone, H.A. and Leal, L.G., "Relaxation and breakup of an initially extended drop in an otherwise quiescent fluid," J. Fluid Mech. **198**, 399 (1989).

[42] Stuart, J.T., "On the nonlinear mechanics of wave disturbances in stable and unstable parallel flows. Part 1. The basic behaviour for plane Poiseuille flow," J. Fluid Mech. **9**, 353 (1960).

[43] Taylor, G.I., "The dynamics of thin sheets of fluid, I. Water bells," Proc. R. Soc. London Ser. A **253**, 289 (1959).

[44] Ting, L. and Keller, J.B., "Slender jets and thin sheets with surface tension," SIAM J. Appl. Math. **50** No. 6, 1533 (1990).

[45] Tjahjadi, M., Stone, H.A. and Ottino, J.M., "Satellite and subsatellite formation in capillary breakup," J. Fluid Mech. **243**, 297 (1992).

[46] Watson, J., "On the nonlinear mechanics of wave disturbances in stable and unstable parallel flows. Part 2. The development of a solution for plane Poiseuille flow and plane Couette flow," J. Fluid Mech. **9**, 371 (1960).

[47] Whitham, G.B., *Linear and Nonlinear Waves*, Wiley-Interscience, New York (1974).

[48] Yuen, M.-C., "Nonlinear capillary instability of a liquid jet," J. Fluid Mech. **33**, 151 (1968).

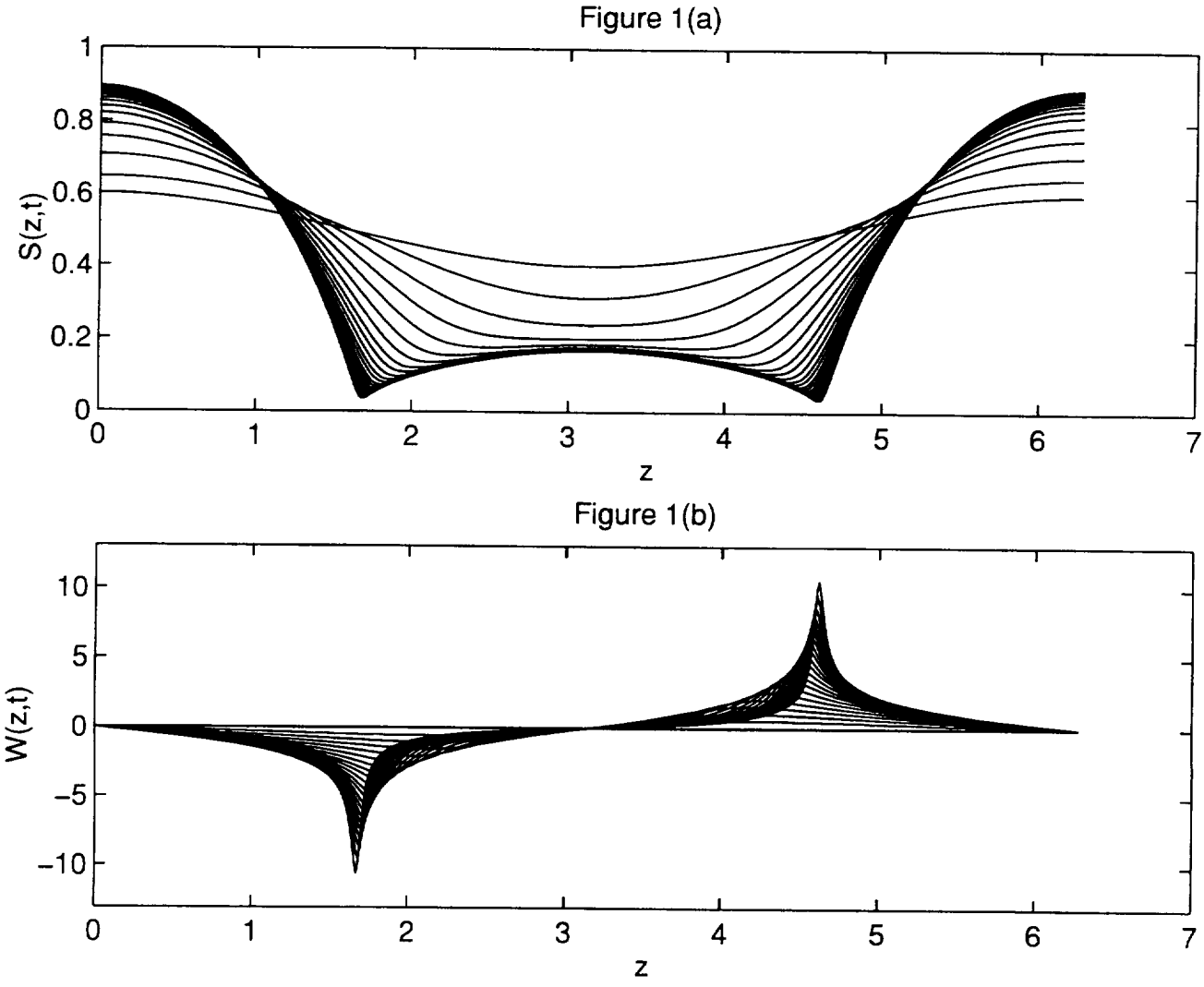

FIGURE 1 Inviscid slice model, evolution to drop formation. (a) Jet shape; (b) Axial velocity.

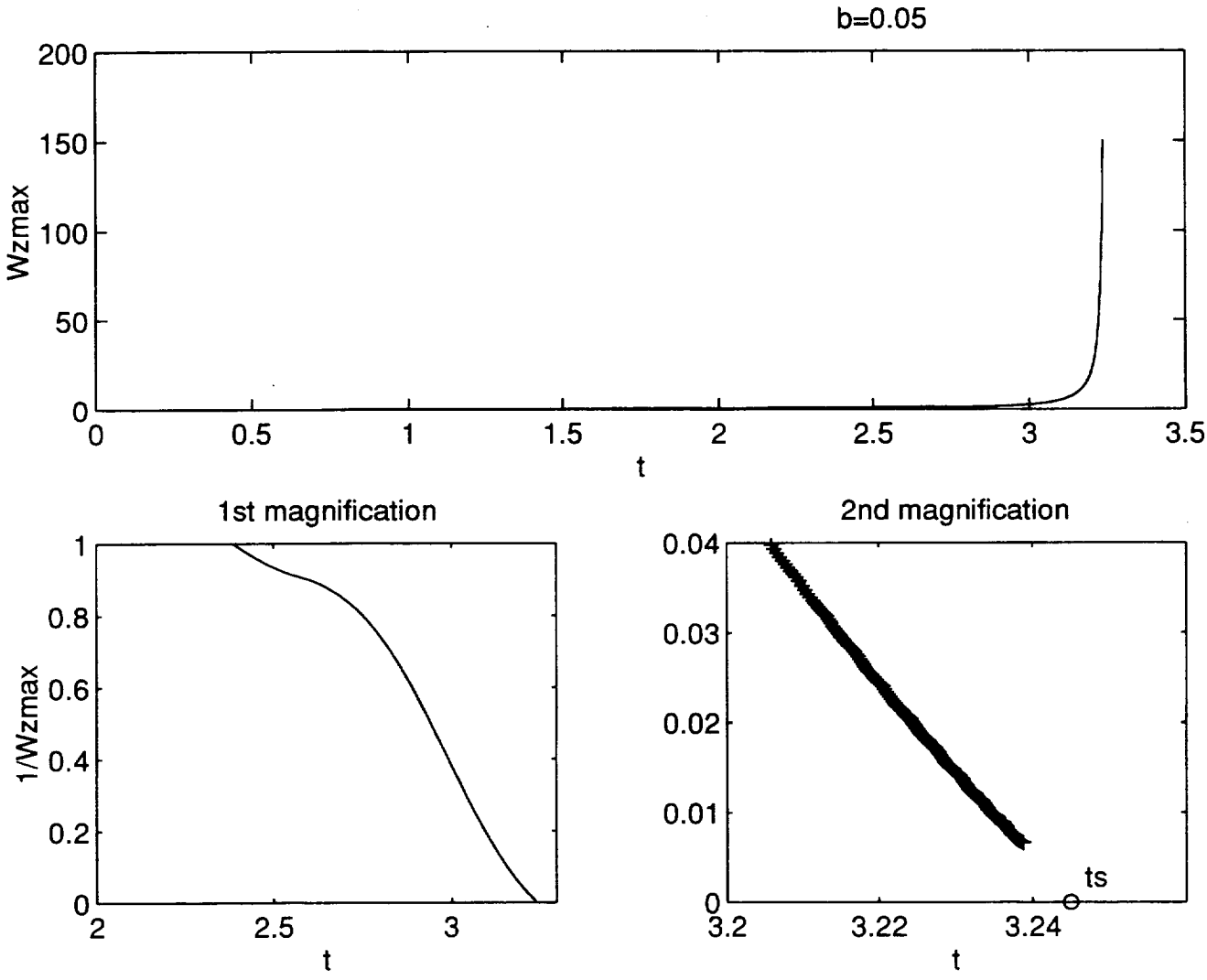

FIGURE 2 Estimation of singular times for inviscid slice model runs.

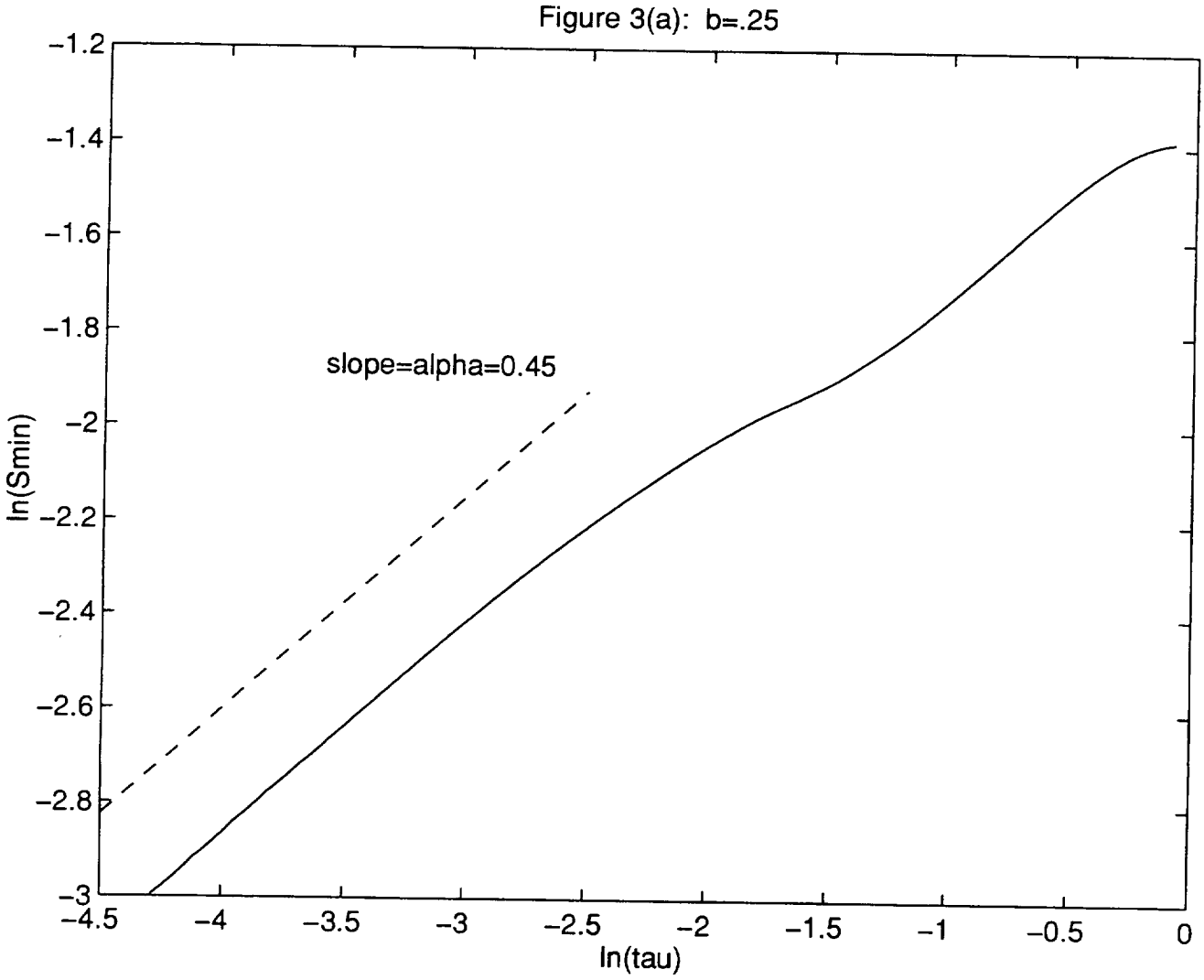

FIGURE 3 Inviscid slice model. Estimation of the scaling exponents. (a) Exponent α; (b) Exponent β.

Figure 3(b): b=0.25

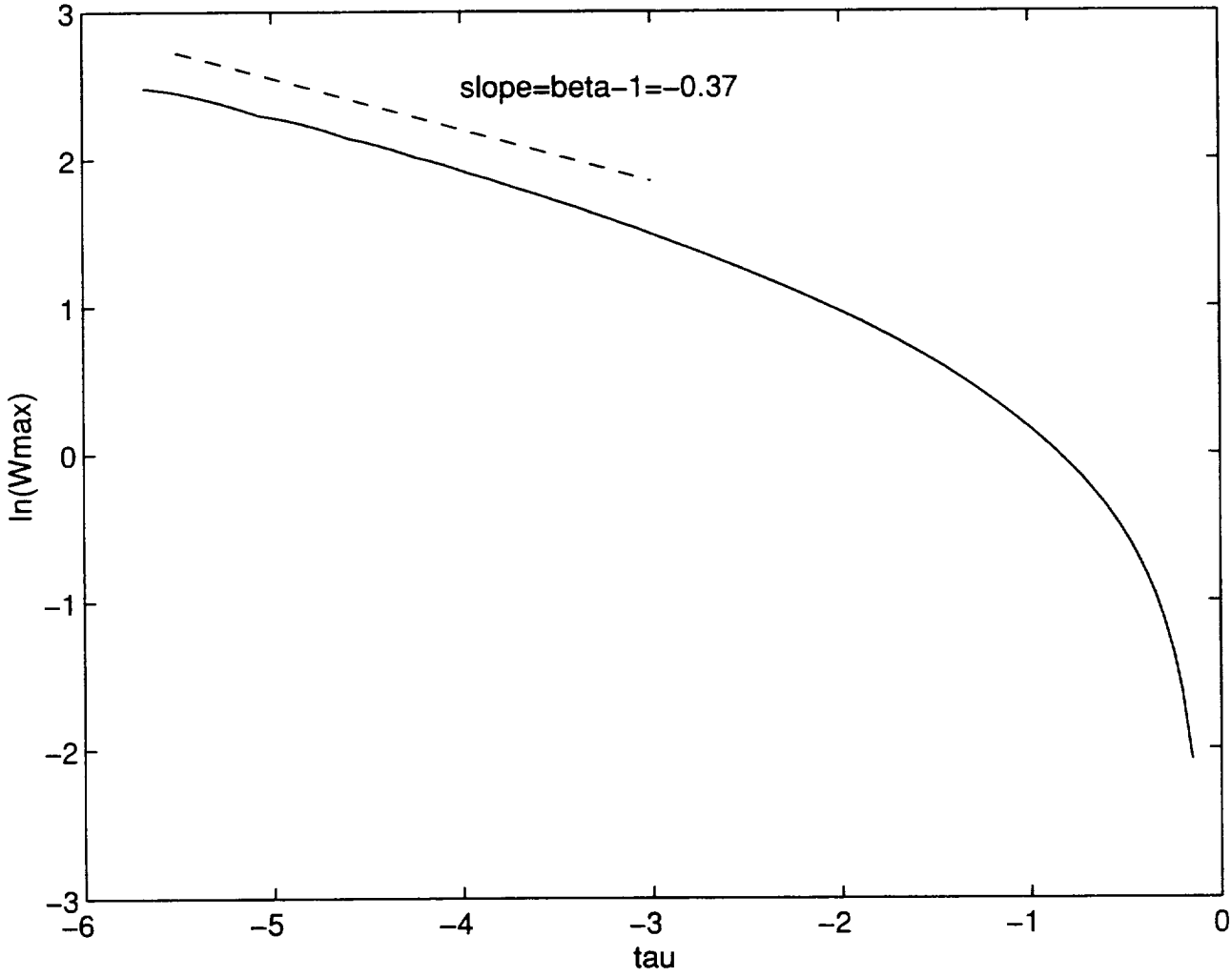

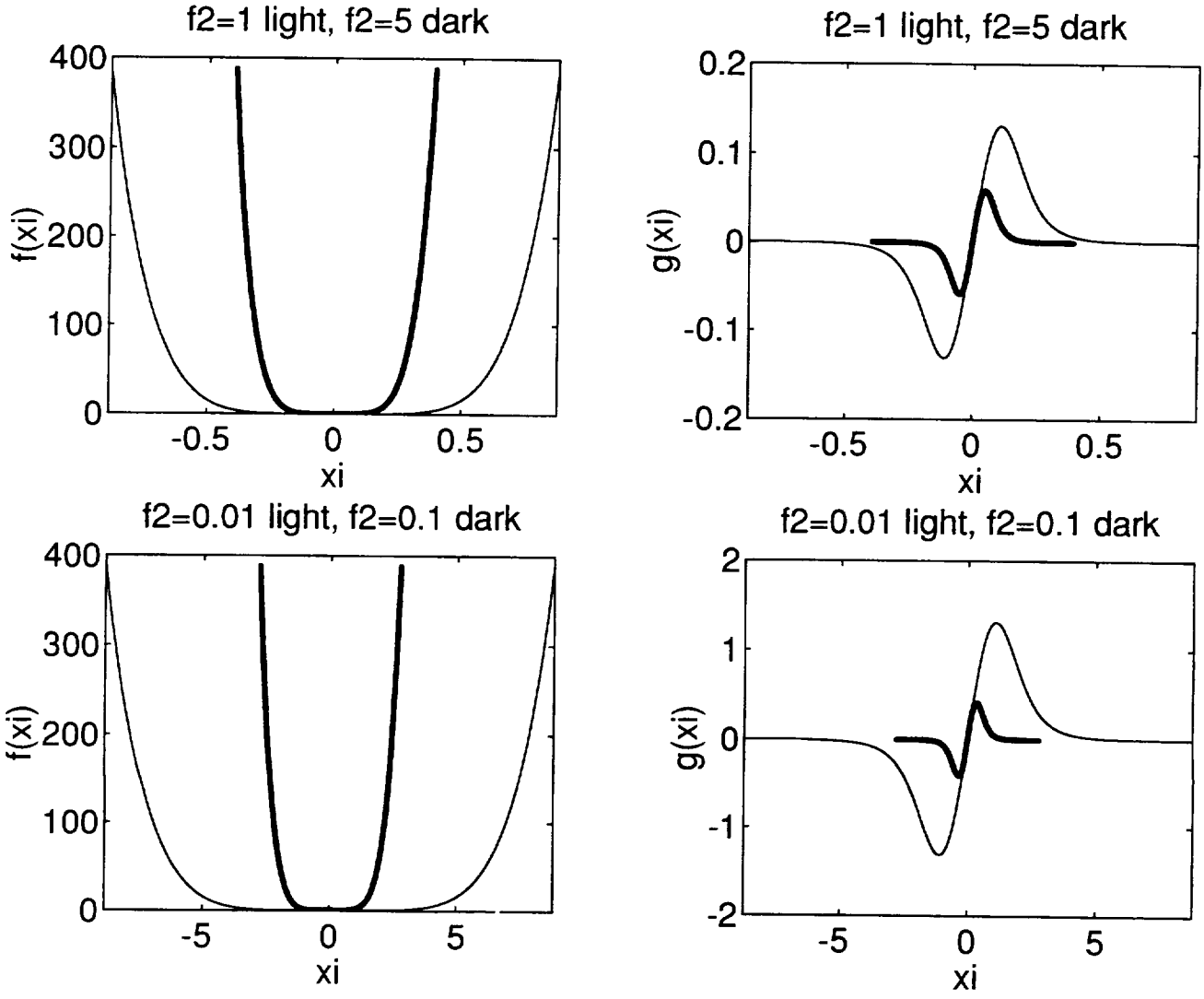

FIGURE 4 Stokes jets. Similarity scaling functions $f(\xi)$ and $g(\xi)$ for different values of the parameter f_2.

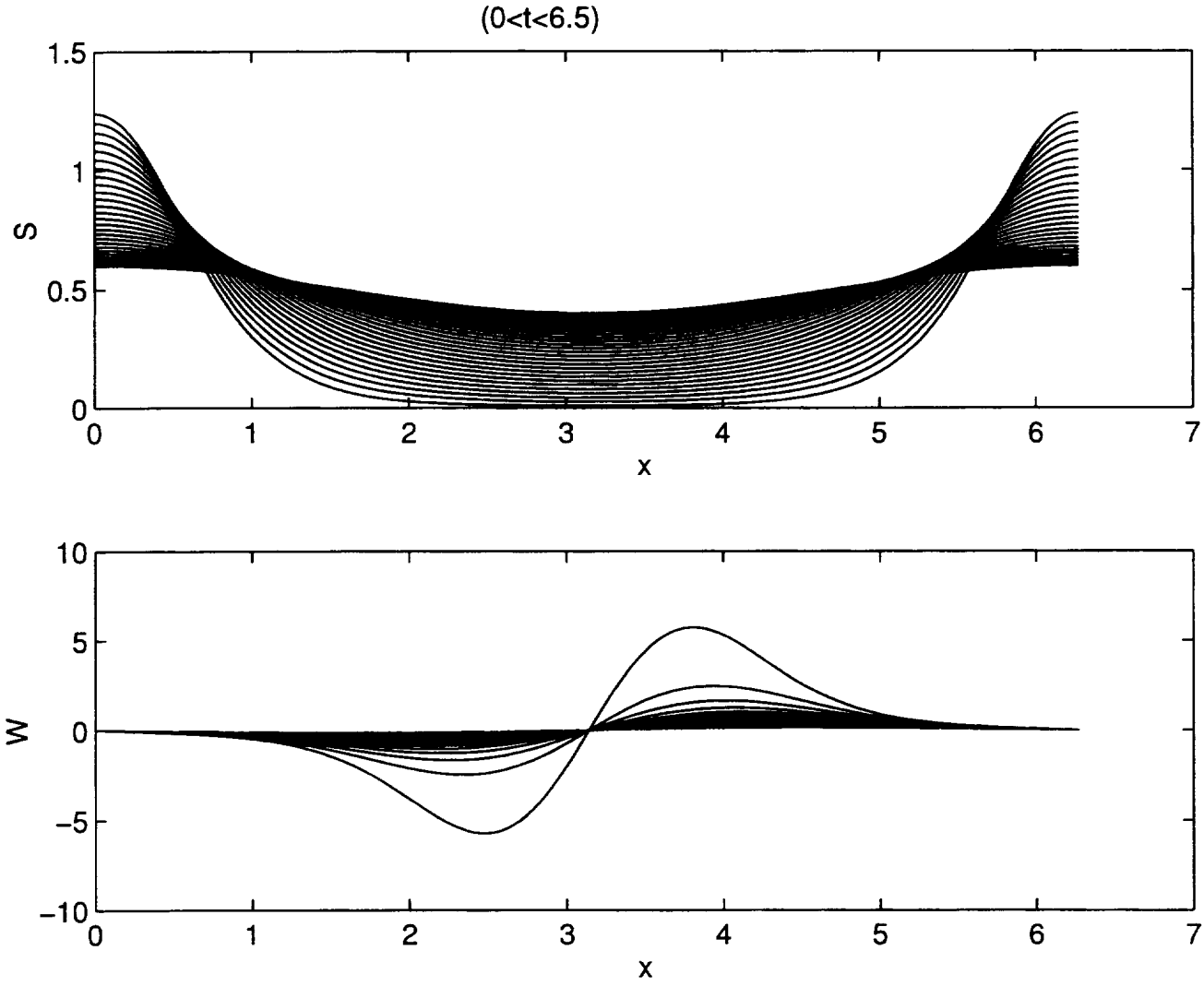

FIGURE 5 Simulation using 1-D Stokes model. Evolution of the jet shape, $S(z,t)$, and the axial velocity, $W(z,t)$.

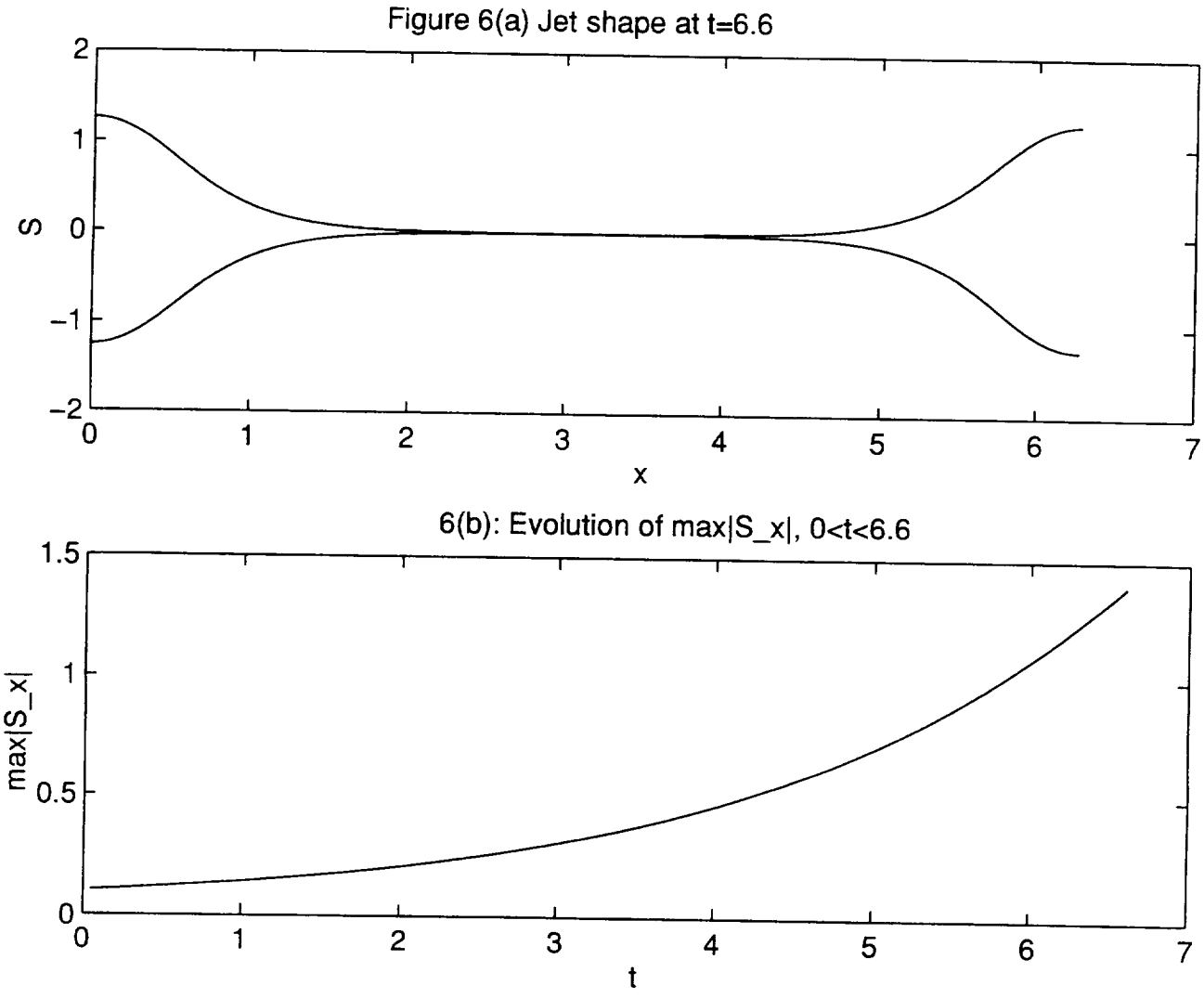

FIGURE 6 Simulation using 1-D Stokes model. Computed jet shape near the singular time and variation of the maximum interfacial slope with time (boundedness shows validity of the slender jet approximation).

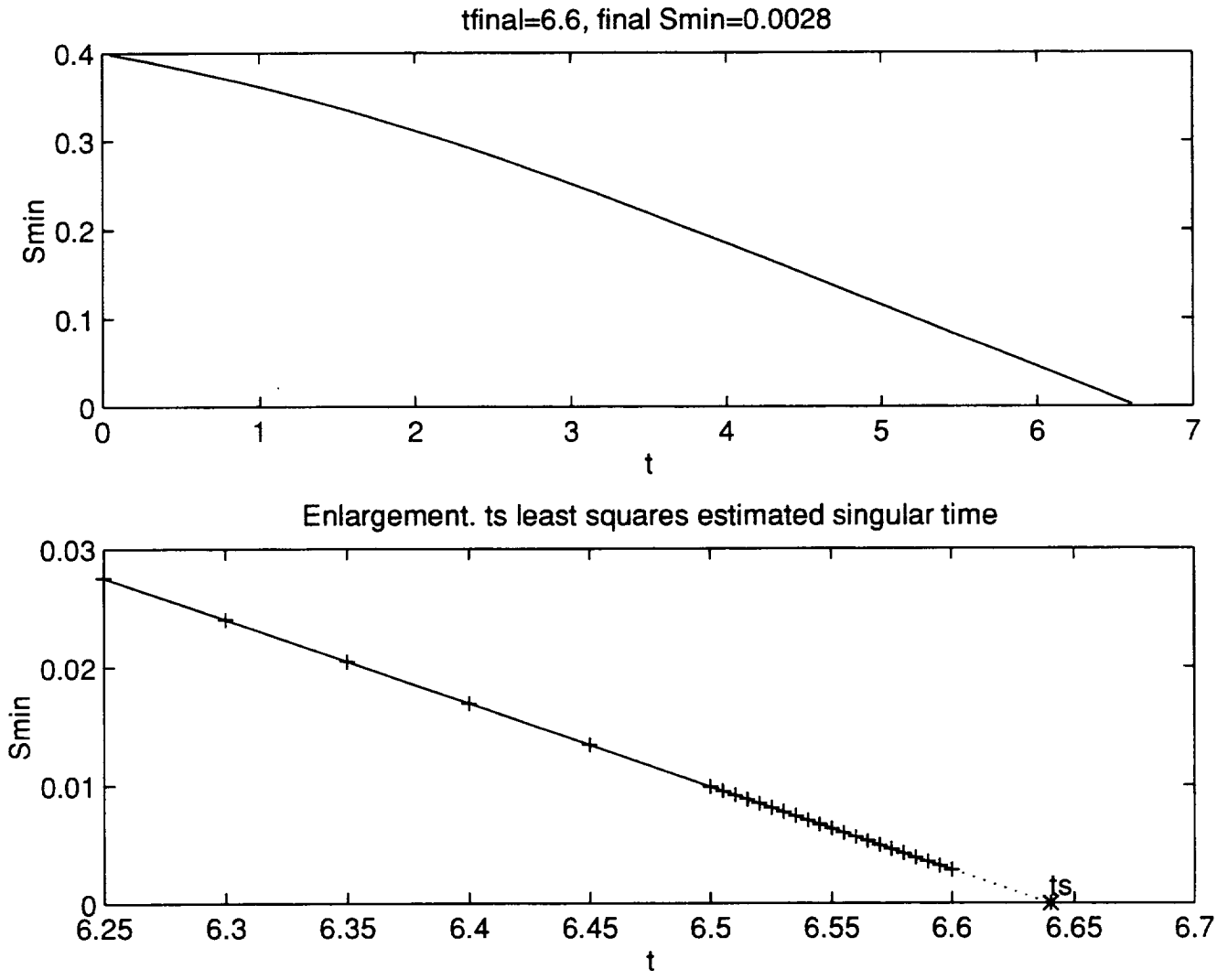

FIGURE 7 Simulation using 1-D Stokes model. Time history of $S_{min}(t)$ along with an enlargement outlining the estimation of the singular time, t_s.

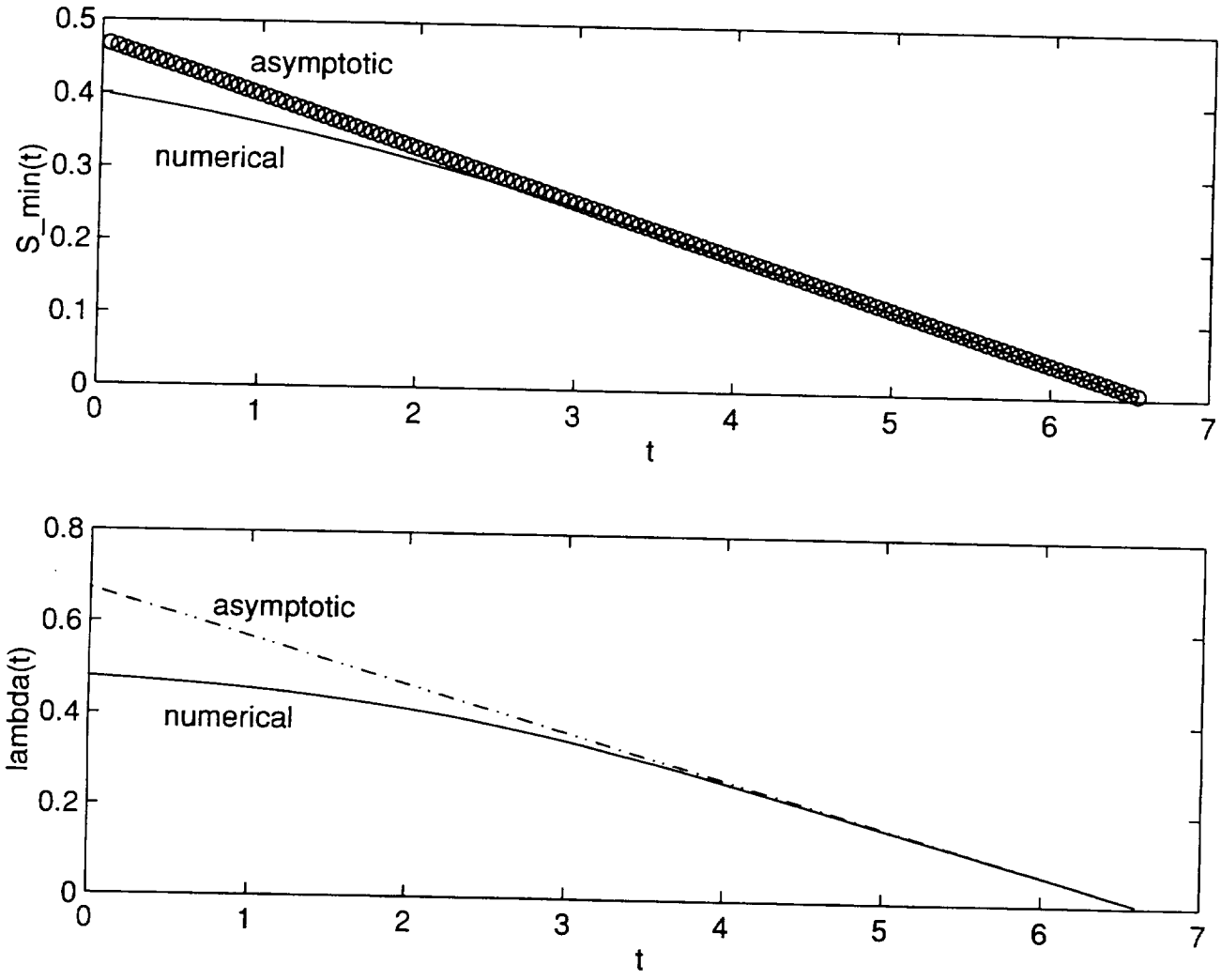

FIGURE 8 Simulation using 1-D Stokes model. Comparison of theory and simulation as $t \rightarrow t_s$ for the evolution of $S_{min}(t)$ and the force in the jet, $\lambda(t)$.

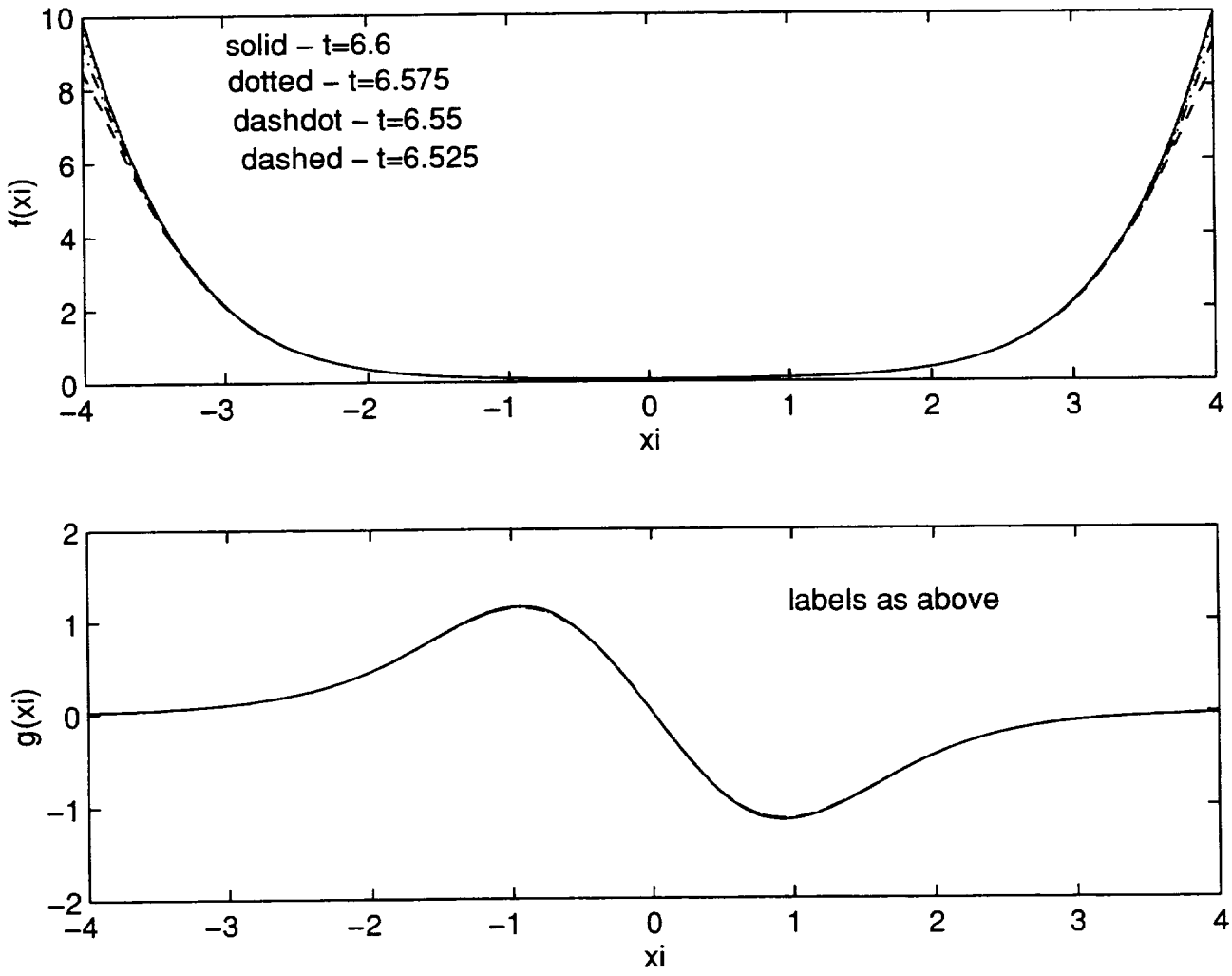

FIGURE 9 Simulation using 1-D Stokes model. Convergence to a scaling function as $t \to t_s$. (a) The scaling function $f(\xi)$, (b) $g(\xi)$.

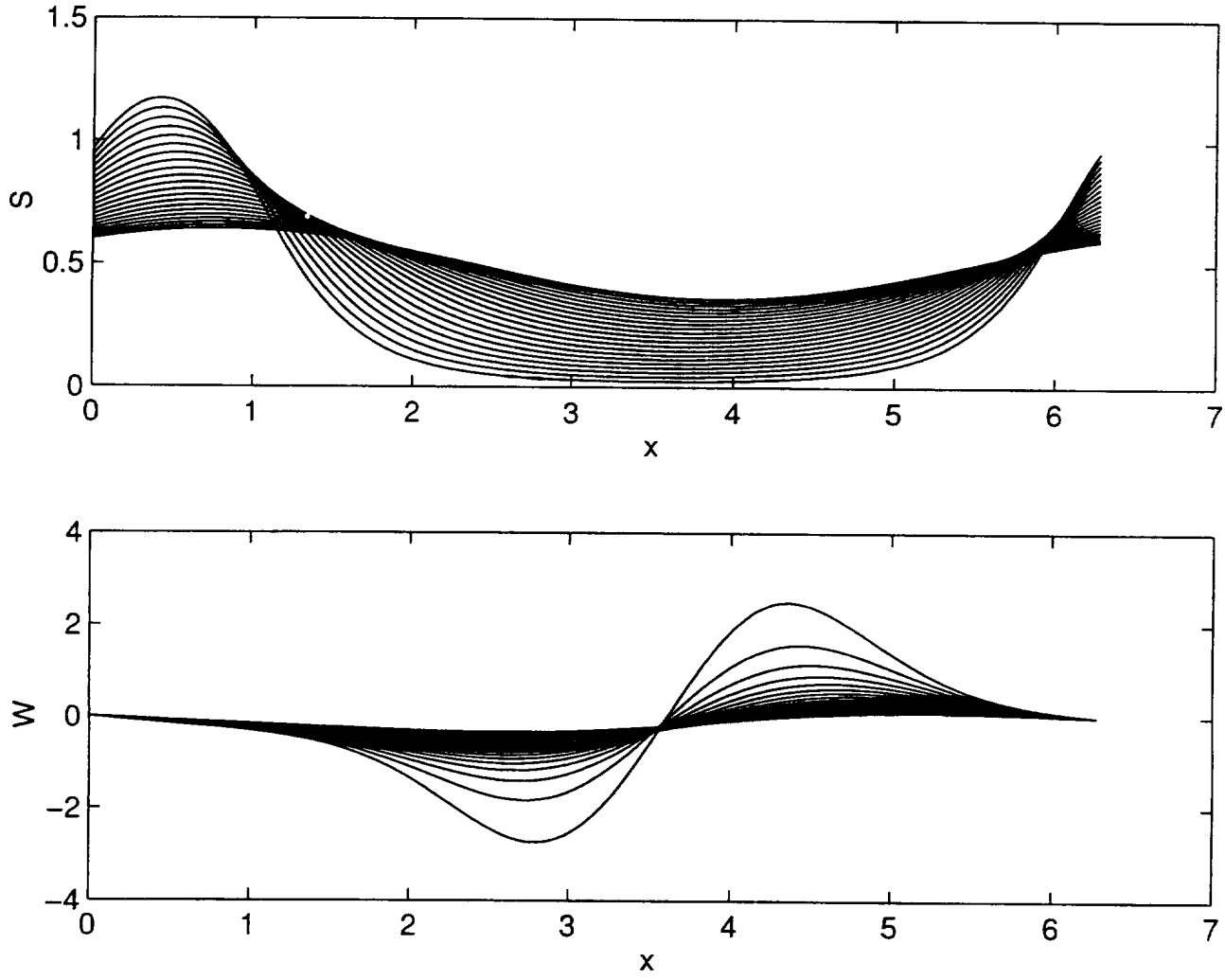

FIGURE 10 Simulation using 1-D Stokes model. Non-symmetric initial conditions. Evolution of $S(z,t)$ and $W(z,t)$.

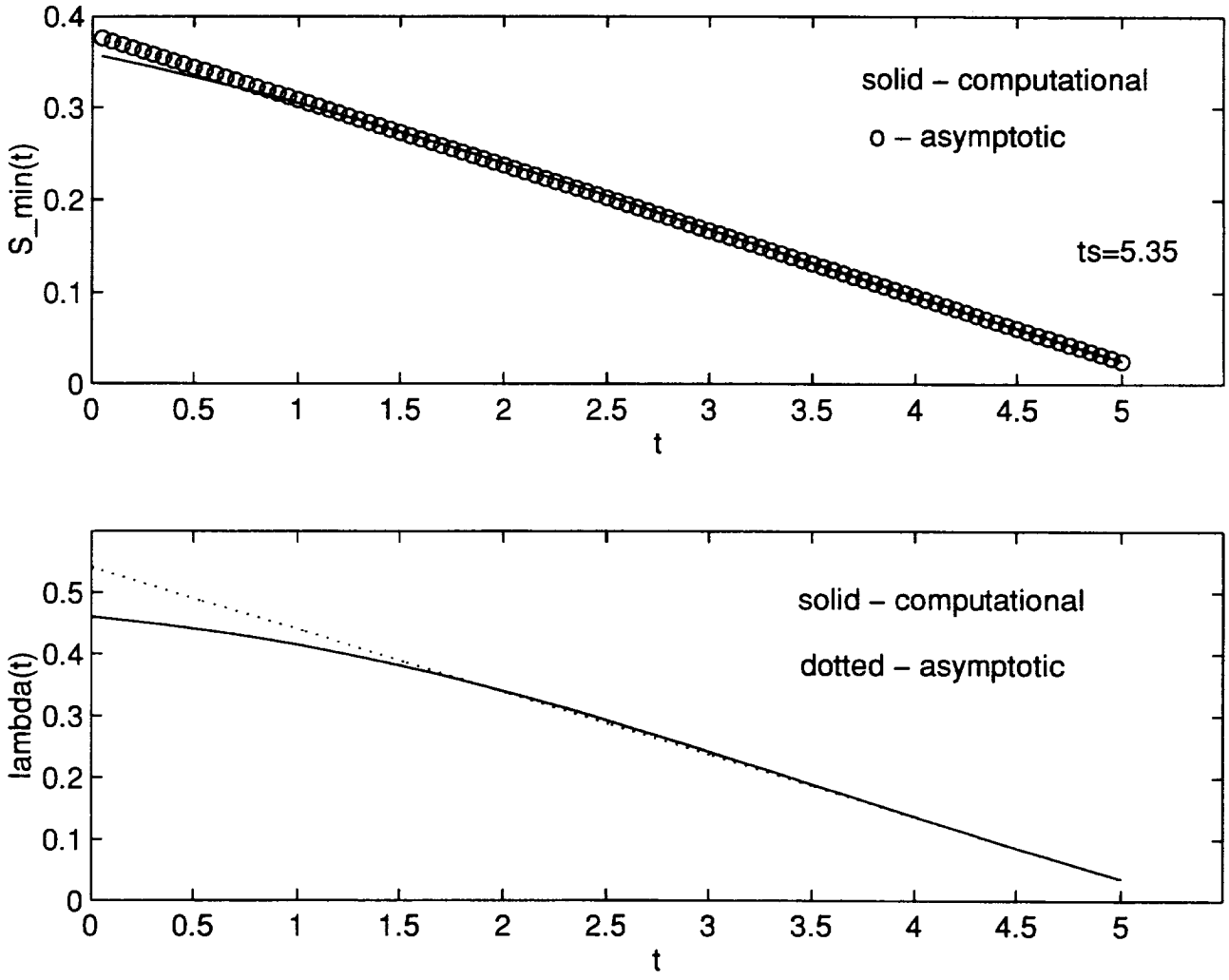

FIGURE 11 Non-symmetric initial conditions. Comparison between theory and computation for the evolution of (a) $S_{min}(t)$, and, (b) $\lambda(t)$.

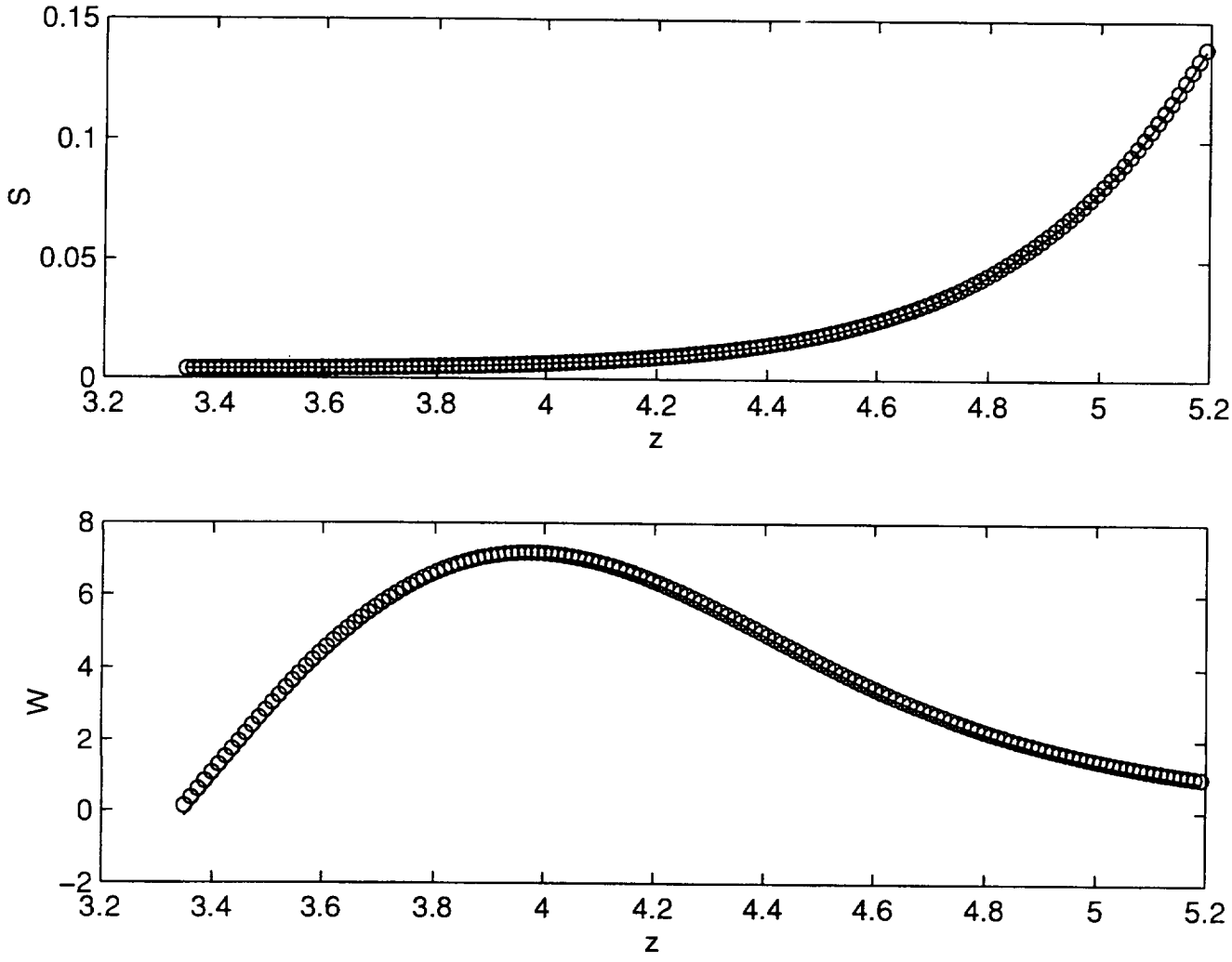

FIGURE 12 Non-symmetric initial conditions. Symmetry of solutions near the breakup point.

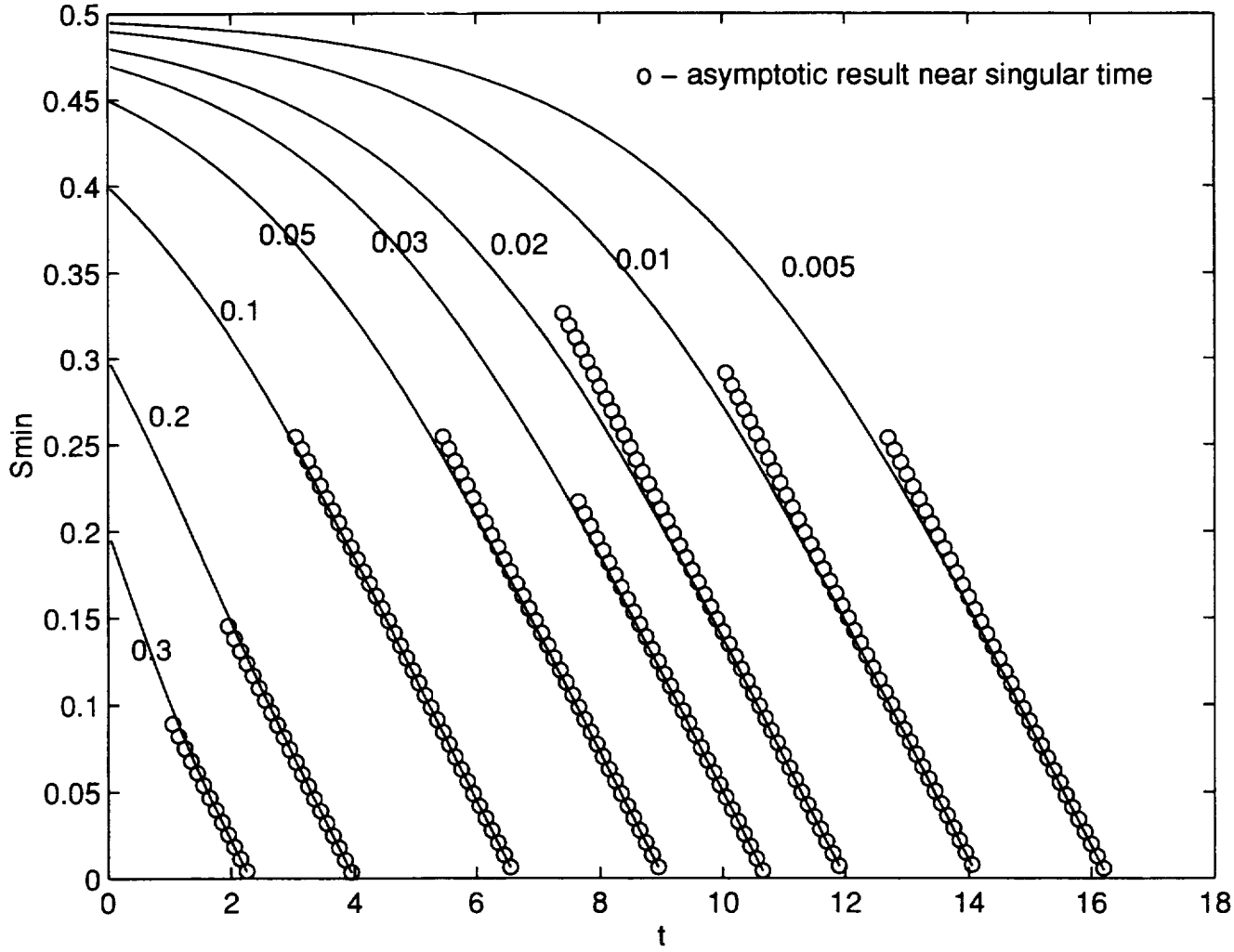

FIGURE 13 Symmetric initial conditions. Evolution of $S_{min}(t)$ for different initial conditions. The theoretical predictions (valid as $t \rightarrow t_s$) are also included.

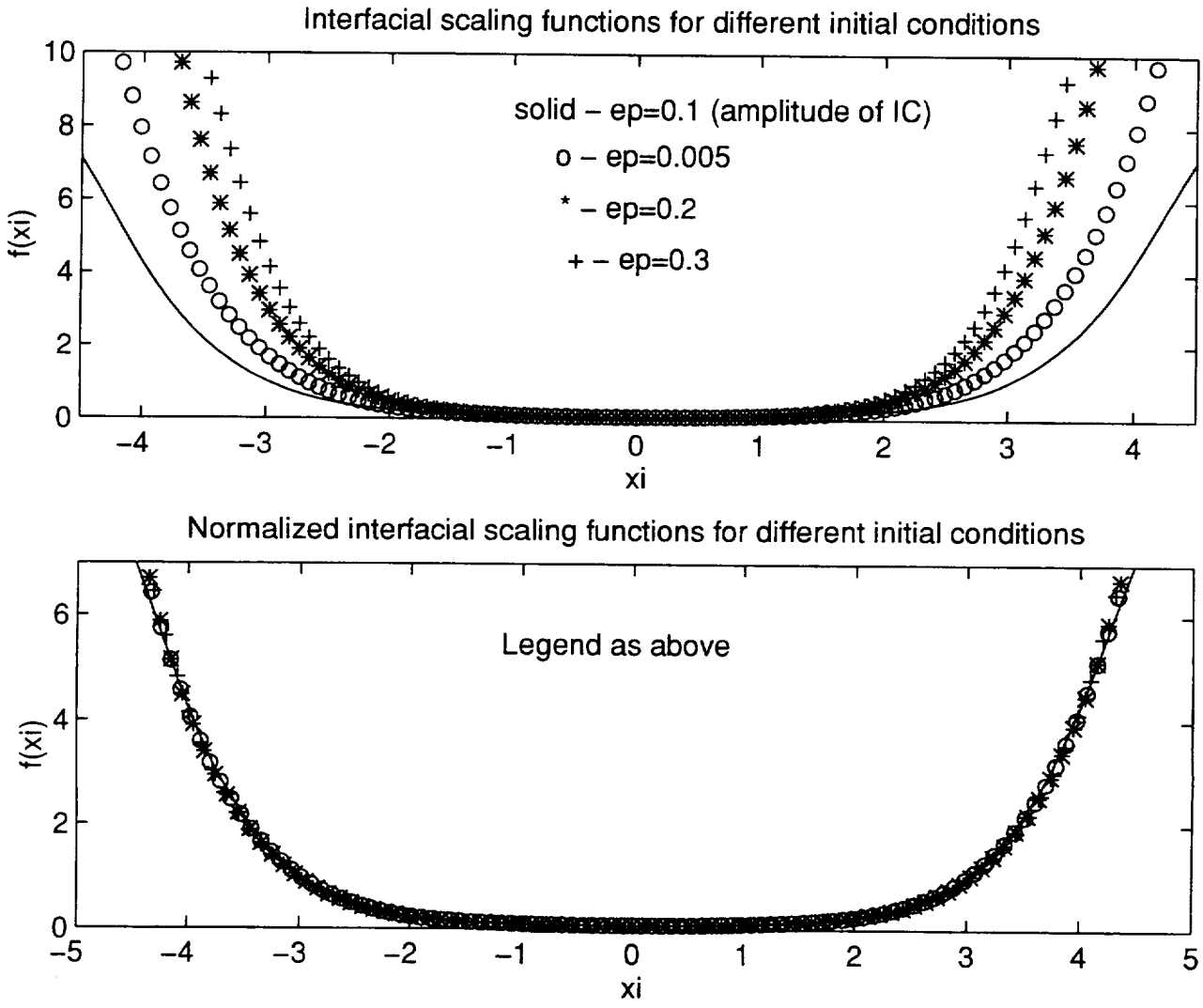

FIGURE 14 Symmetric initial conditions. Interfacial similarity scaling functions for different initial conditions. The lower graph shows the construction of a universal scaling function by a linear axial transformation.

REPORT DOCUMENTATION PAGE

Form Approved
OMB No. 0704-0188

1. AGENCY USE ONLY *(Leave blank)*	2. REPORT DATE	3. REPORT TYPE AND DATES COVERED
	March 1996	Contractor Report

4. TITLE AND SUBTITLE
DESCRIPTION OF JET BREAKUP

5. FUNDING NUMBERS
C NAS1-19480
WU 505-90-52-01

6. AUTHOR(S)
Demetrios T. Papageorgiou

7. PERFORMING ORGANIZATION NAME(S) AND ADDRESS(ES)
Institute for Computer Applications in Science and Engineering
Mail Stop 132C, NASA Langley Research Center
Hampton, VA 23681-0001

8. PERFORMING ORGANIZATION REPORT NUMBER
ICASE Report No. 96-17

9. SPONSORING/MONITORING AGENCY NAME(S) AND ADDRESS(ES)
National Aeronautics and Space Administration
Langley Research Center
Hampton, VA 23681-0001

10. SPONSORING/MONITORING AGENCY REPORT NUMBER
NASA CR-198294
ICASE Report No. 96-17

11. SUPPLEMENTARY NOTES
Langley Technical Monitor: Dennis M. Bushnell
Final Report
To appear in Advances in Multi-Fluid Flows.

12a. DISTRIBUTION/AVAILABILITY STATEMENT
Unclassified–Unlimited

Subject Category 34

12b. DISTRIBUTION CODE

13. ABSTRACT *(Maximum 200 words)*
In this article we review recent results on the breakup of cylindrical jets of a Newtonian fluid. Capillary forces provide the main driving mechanism and our interest is in the description of the flow as the jet pinches to form drops. The approach is to describe such topological singularities by constructing local (in time and space) similarity solutions from the governing equations. This is described for breakup according to the Euler, Stokes or Navier-Stokes equations. It is found that slender jet theories can be applied when viscosity is present, but for inviscid jets the local shape of the jet at breakup is most likely of a non-slender geometry. Systems of one-dimensional models of the governing equations are solved numerically in order to illustrate these differences.

14. SUBJECT TERMS
capillary instability; finite-time singularities; self-similar solutions

15. NUMBER OF PAGES
39

16. PRICE CODE
A03

17. SECURITY CLASSIFICATION OF REPORT	18. SECURITY CLASSIFICATION OF THIS PAGE	19. SECURITY CLASSIFICATION OF ABSTRACT	20. LIMITATION OF ABSTRACT
Unclassified	Unclassified		